No detectable influence of the carbonate ion effect on changes in stable carbon isotope ratios (δ^{13}C) of shallow dwelling planktic foraminifera over the past 160 kyr

Peter Köhler[1] and Stefan Mulitza[2]

[1]Alfred-Wegener-Institut Helmholtz-Zentrum für Polar-und Meeresforschung (AWI), Bremerhaven, Germany
[2]MARUM — Center for Marine Environmental Sciences and Faculty of Geosciences, University of Bremen, Germany

Correspondence: Peter Köhler (peter.koehler@awi.de)

Version: March 4, 2024

Abstract. Laboratory experiments showed that the isotopic fractionation of δ^{13}C and of δ^{18}O during calcite formation of planktic foraminifera are species-specific functions of ambient CO_3^{2-}-concentration. This effect became known as the carbonate ion effect (CIE), whose role for the interpretation of marine sediment data will be investigated here in an in-depth analysis of the ^{13}C cycle. For that effort we constructed new 160 kyr-long mono-specific stacks of changes in both δ^{13}C and δ^{18}O from either the planktic foraminifera *Globigerinoides ruber* (rub) or *Trilobatus sacculifer* (sac) from 112 and 40 marine records from the wider tropics (latitudes below 38°), respectively. Both mono-specific time series $\Delta(\delta^{13}C_{rub})$ and $\Delta(\delta^{13}C_{sac})$ are very similar to each other and a linear regression through a scatter plot of both data sets has a slope of ∼0.99 — although the laboratory-based CIE for both species differ by nearly a factor of two, implying that they should record distinctly different changes in δ^{13}C, if we accept that the carbonate ion concentration changes on glacial/interglacial timescales. For a deeper understanding of the ^{13}C cycle we use the global carbon cycle model BICYCLE-SE to calculate how surface ocean CO_3^{2-} should have varied over time in order to be able to calculate the potential offsets which would by caused by the CIE quantified in culture experiments. Our simulations are forced with atmospheric reconstructions of CO_2 and $\delta^{13}CO_2$ derived from ice cores to obtain a carbon cycle which should at least at the surface ocean be as close as possible to expected conditions and which in the deep ocean largely agrees with the carbon isotope ratio of dissolved inorganic carbon (DIC), $\delta^{13}C_{DIC}$, as reconstructed from benthic foraminifera. We find that both $\Delta(\delta^{13}C_{rub})$ and $\Delta(\delta^{13}C_{sac})$ agree better with changes in simulated $\delta^{13}C_{DIC}$ when ignoring the CIE than those time series which where corrected for the CIE. The combination of data- and model-based evidence for the lack of a role for the CIE in $\Delta(\delta^{13}C_{rub})$ and $\Delta(\delta^{13}C_{sac})$ suggests that the CIE as measured in laboratory experiments is not directly transferable to the interpretation of marine sediments records. The much smaller CIE-to-glacial/interglacial-signal-ratio in foraminifera δ^{18}O, when compared to δ^{13}C, prevents us to draw robust conclusions on the role of the CIE on δ^{18}O as recorded in the hard shells of both species. However, theory proposes that the CIE in δ^{13}C and δ^{18}O depends both on the pH in the surrounding water, suggesting that the CIE should be detectable in neither or both of the isotopes. Whether this lack of role of the CIE in the interpretation of planktic paleo data is a general feature, or restricted to the two species investigated here, needs to be checked with further data from other planktic foraminiferal species.

1 Introduction

For a reconstruction of past changes in the ocean and the carbon cycle various variables are measured on microfossils obtained from marine sediment cores. Among the most widley used are the stable carbon and oxygen isotope ratios, δ^{13}C and δ^{18}O, from hard shells of planktic and benthic foraminifera. Since the publication of the first stable isotope time series (Emiliani, 1955) a vast number of of stable isotope records has been published and to a large part compiled in the World Atlas of late Quaternary Foraminiferal Oxygen and Carbon Isotope Ratios (Mulitza et al., 2022). One of the fundamental problems with the interpretation of foraminiferal isotope ratios is how and why was a stable isotope signal altered on its way from the sea water to the shell of living foraminifera. Are there vital and other effects necessary to be considered when interpreting the paleo records (e.g. Bijma et al., 1999; Zeebe et al., 2008; Kimoto, 2015)?

The carbonate ion effect (CIE) is one of these potentially important effects that might alter the isotopic signal. The CIE implies that both δ^{13}C and δ^{18}O measured in hard shells of marine organisms undergo isotopic fractionation during calcite formation with the amplitude of the fractionation, among other factors, being a function of the carbonate ion concentration ($[CO_3^{2-}]$) of the surrounding seawater (Spero et al., 1997). The CIE has been found to be species-specific (Spero et al., 1999), ranging from -4.7 to -13.0×10^{-3} ‰ per μmol kg^{-1} of $[CO_3^{2-}]$ for δ^{13}C and between -1.4 and -4.5×10^{-3} ‰ per μmol kg^{-1} of $[CO_3^{2-}]$ for δ^{18}O in four planktic foraminifera. The CIE for δ^{13}C has been explained for *Orbulina universa*, a spinose, symbiont bearing species, by the pH-related distribution of dissolved inorganic carbon (DIC) into its three species CO_2, CO_3^{2-}, and HCO_3^- (Wolf-Gladrow et al., 1999; Zeebe et al., 1999). The CIE on δ^{18}O is also explained by the CO_3^{2-}-related varying pH (Zeebe, 1999). These theories, however, were unable to base the full amplitudes found in experiments solely on this effect. The CIE is maybe the most prominent isotopic fractionation effect which has to be considered when interpreting the paleo records, but others, e.g vital effects and dependency on light, temperature, pressure and shell size, have been put forward (e.g. Spero and Williams, 1988, 1989; Spero et al., 1991; Spero, 1992; Spero and Lea, 1993; Oppo and Fairbanks, 1989). The CIE is found to play a minor role when comparing late Holocene deep ocean δ^{13}C in benthic foraminifera with δ^{13}C of DIC ($\delta^{13}C_{DIC}$) (Schmittner et al., 2017) being responsible for -2.6×10^{-3} ‰ per μmol kg^{-1} of $[CO_3^{2-}]$ disturbance in the recorded signal. In a recent study focusing on the benthic species *Cibicidoides wuellerstorfi* -3.0×10^{-3} ‰ per μmol kg^{-1} of $[CO_3^{2-}]$ have been obtained for the late Holocene (Nederbragt, 2023). Both studies also found in addition to the CIE that $\delta^{13}C_{benthic}$ was also partly controlled by other variables, mainly pressure (water depth) and temperature.

The CIE in planktic foraminifera is one of the reasons why the interpretation of the whole δ^{13}C cycle over glacial/interglacial timescales is still challenging. In a compilation of foraminiferal $\delta^{13}C$ measurements covering the past 150 kyrs, Oliver et al. (2010) find relatively large disagreements between different planktic $\delta^{13}C$ records within a region, compared to benthic records, consistent with large uncertainty attributed to the estimation of $\delta^{13}C_{DIC}$ from planktic species. Since benthic compilations are less affected by the CIE, they should, however, robustly constrain deep ocean changes in $\delta^{13}C_{DIC}$. A more recent compilation of benthic δ^{13}C was given in Lisiecki (2014). Furthermore, δ^{13}C of atmospheric CO_2 ($\delta^{13}CO_2$) is now available over the last 155 kyr (Eggleston et al., 2016a) from ice cores. Missing in our understanding are so far tight constraints on change in surface

ocean $\delta^{13}C_{DIC}$, but in principle this information should be recorded in the hard shells of planktic foraminifera, even if hidden under the CIE.

We therefore here aim to construct a robust time series of orbital changes in surface ocean $\delta^{13}C_{DIC}$ based on planktic foraminifera data. We compiled $\delta^{13}C$ data largely based on Mulitza et al. (2022) covering up to the last 160 kyr. In order to be able to apply any species-specific CIE corrections we compile mono-specific isotope records on the widely abundant shallow-dwelling planktic foraminifera species *Globigerinoides ruber* (*G. ruber* or rub) and *Trilobatus sacculifer* (*T. sacculifer* or sac) into stacks. Due to their spatial distribution (Fraile et al., 2008) this species selection leads effectively to the construction of $\Delta(\delta^{13}C_{rub})$ and $\Delta(\delta^{13}C_{sac})$ stacks based on sediment core data from the latitudes smaller than 40°, potentially informing us about mean changes of $\delta^{13}C_{DIC}$ on orbital timescales in the surface of the wider tropical ocean. Accompanied stacks of $\Delta(\delta^{18}O_{rub})$ and $\Delta(\delta^{18}O_{sac})$ from the same cores will add further information on the CIE in $\delta^{18}O$.

A first surface ocean $\delta^{13}C$ stack based on data from *T. sacculifer* obtained from five equatorial Atlantic records has been constructed by Curry and Crowley (1987) without any knowledge on the CIE. Furthermore, Spero et al. (1999) used data from *G. ruber* and *T. sacculifer* from a single core in the Indian Ocean and the lab-based size of their species-specific CIE to deconvolve surface ocean $[CO_3^{2-}]$. We here will use our new mono-specific $\delta^{13}C$ stacks, which have due to the underlying number of records a much higher signal-to-noise-ratio to test the robustness of their findings.

In the following we will investigate the connection of $\delta^{13}C$ in atmosphere and ocean in closer detail in order to improve our understanding of the ^{13}C cycle. The remainder of the article is structured as follows. We first (section 2.1) describe the construction of our mono-specific $\delta^{13}C$ anomaly stacks $\Delta(\delta^{13}C_{rub})$ and $\Delta(\delta^{13}C_{sac})$ (and of the accompanied $\delta^{18}O$ anomalies). Some published benthic $\delta^{13}C$ data are also needed for our understanding (section 2.2). For a deeper interpretation the global isotope enabled carbon cycle model BICYCLE-SE (Köhler and Munhoven, 2020), which has been proven to simulate glacial/interglacial (G/IG) changes in the carbon cycle reasonably well, is used. The model is briefly described in section 2.3 including a completely revised parametrisation of the ^{13}C cycle. We then first discuss (section 3.1) what we already know from data on the $\delta^{13}C$ cycle and the role the CIE might play. We then analyse in section 3.2 the simulated $\delta^{13}C$ cycle in our model results. This enables us to evaluate (section 3.3) if our stacks $\Delta(\delta^{13}C_{rub})$ and $\Delta(\delta^{13}C_{sac})$ are good representations of changes in $\delta^{13}C_{DIC}$ in the wider tropical surface ocean or if corrections such as the CIE need to be applied. Finally, we briefly discuss the CIE in $\delta^{18}O_{rub}$ and $\delta^{18}O_{sac}$ (section 3.4), before we come to our conclusions (section 4).

2 Methods

2.1 Constructing new mono-specific stacks from planktic foraminifera

Data source and age modelling: To construct time series of low-latitude $\delta^{13}C$ variations through the past 160 kyr, we selected 112 and 40 $\delta^{13}C$ records of the shallow-dwelling planktic foraminifera *G. ruber* and *T. sacculifer*, respectively, predominantely from the World Atlas of late Quaternary Foraminiferal Oxygen and Carbon Isotope Ratios (Mulitza et al., 2022). A list of the isotope records contributing to our stacks with relevant meta data, references to the original publications and data sources is provided in Table S1. In three sediment cores time series from both *G. ruber white* and *G. ruber pink* contribute to our *G.*

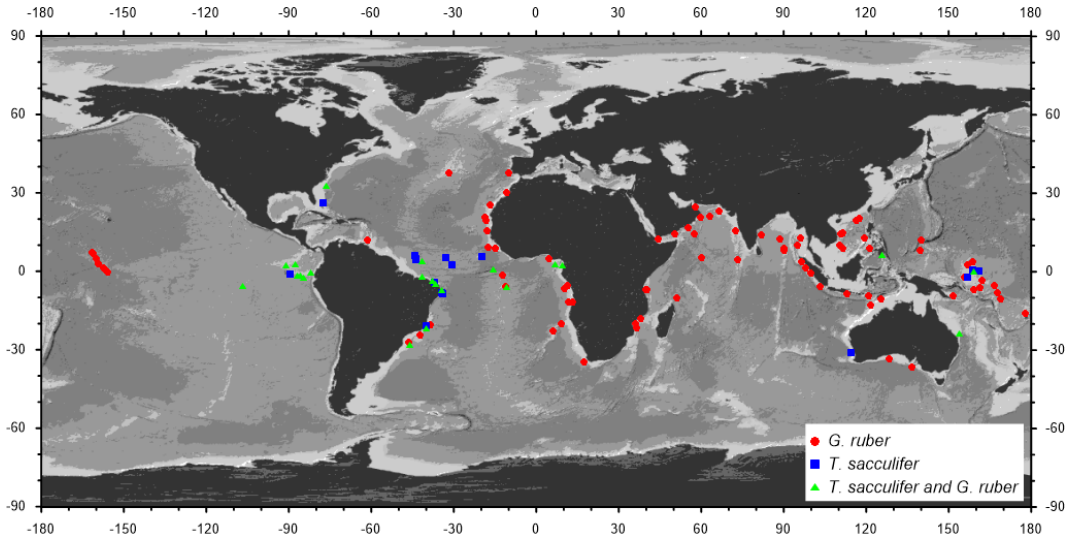

Figure 1. Location of the 127 sediment cores from which data have been compiled for this study. In 87 cores data from the planktic species *G. ruber* and in 18 cores data from *T. sacculifer* have been included, while 22 cores provided mono-specific data from both species.

ruber stacks, while data from 22 cores contain mono-specific data from both *G. ruber* and *T. sacculifer*. All combined our data selection is based on material from 127 sediment cores. The core sites cover a latitudinal range from 37.6°N to 36.7°S for *G. ruber* and of 32.8°N to 31.3°S for *T. sacculifer* in all major ocean basins (Figure 1), although the contributions from individual cores (and therefore the latitudinal range) changed over time (Figure 2c). Our age models are based on either radiocarbon ages or oxygen isotope stratigraphy or a combination of both methods. To calibrate radiocarbon ages, we first subtracted a simulated local reservoir age from the nearest grid-box of the modelling experiments conducted for Marine20 (Butzin et al., 2020; Heaton et al., 2020) and then calibrated the corrected radiocarbon age with the IntCal20 calibration curve (Reimer et al., 2020). For core sections with insufficient radiocarbon coverage or outside the radiocarbon dating range ages were added through the visual alignment with the isotope stacks by Lisiecki and Raymo (2005) and Lisiecki and Stern (2016) using the software PaleoDataView (Langner and Mulitza, 2019). In a few cases age models were derived by visual alignment with the oxygen isotope records of well-dated nearby cores. The details of the age model construction are available in the netCDF files of the age models in the corresponding PaleoDataView collection (Köhler and Mulitza, 2023). A continuous age model was then constructed with the age modelling software BACON (Blaauw and Christen, 2011). For each record we produced an ensemble of 1000 time series by combing 1000 BACON-generated age models with 1000 down-core δ^{13}C and δ^{18}O series by adding a random value within the typical analytical 1σ-uncertainty of 0.05% and 0.07‰ to each down-core δ^{13}C and δ^{18}O value, respectively. The resulting 1000 δ^{13}C and δ^{18}O time series were then interpolated to a time step of 1 kyr to calculate the mean and the standard deviation of the time series ensembles. The averaging of the individual ensemble members then led to a considerable smoothing of the final time series.

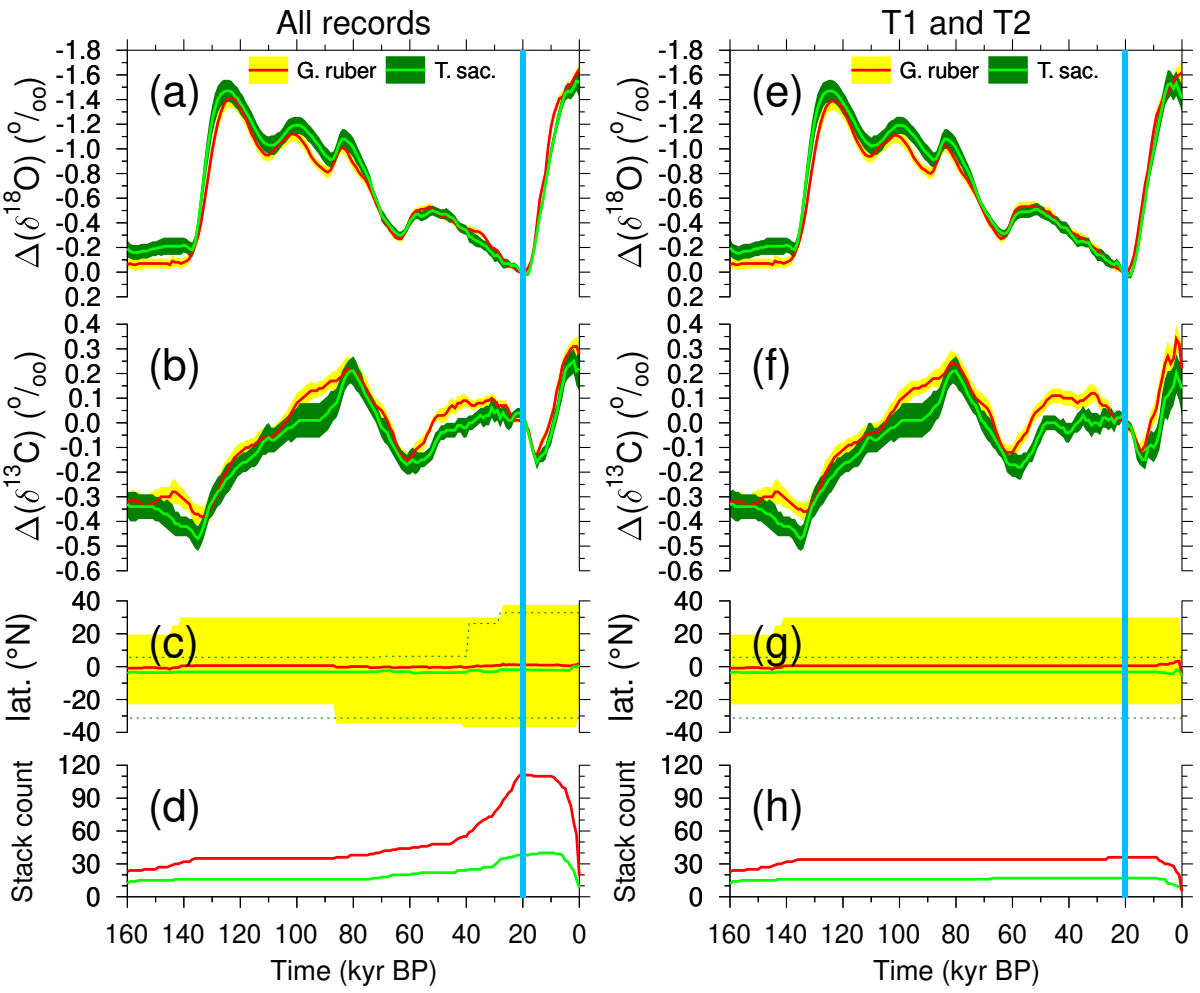

Figure 2. Stacks of anomalies in (a,e) δ^{18}O and (b,f) δ^{13}C from the planktic species *G. ruber* and *T. sacculifer* across the last 160 kyr. Mean anomalies (±1 SE) are calculated with respect to the mean of 21–19 kyr BP (blue vertical band). Data are largely based on Mulitza et al. (2022). (c,g) Latitudinal distribution of cores contributing to the stack (mean and full range) and (d,h) stack count. Either data from all cores for each species are compiled (a–d) or (e–h) from a reduced core selection, in which contributing cores cover both Termination 1 and 2 (T1+T2).

Stacking of down-core isotope records: Although the size class used for stable isotope measurements can vary considerably among records, it is common practice to use a fairly constant size down-core to minimise size-related effects on both oxygen and carbon isotope ratios (e.g. Oppo and Fairbanks, 1989). To provide a common baseline, we corrected all single isotope records by their individual mean values for the period from 21 to 19 kyr BP marked as Last Glacial Maximum (LGM) in various plots. To produce final isotope stacks, we averaged all corrected time series and calculated the standard error (SE) of the means at 1 kyr intervals. The final mono-specific stacks of both δ^{18}O and δ^{13}C anomalies based on *G. ruber* and *T.*

sacculifer are plotted in Figure 2a,b. The oxygen isotope stacks are here also shown to give a clear reference for G/IG changes, δ^{18}O has its maxima during peak glacial times and its minima during peak interglacials. In section 3.4 we will come back to these data to discuss the CIE in $\delta^{18}O_{rub}$ and $\delta^{18}O_{sac}$. To test to what extent the data distribution affects the stacks, we generated two versions of stacks, one based on all records (Figure 2a–d) and an alternative based only on records which contain both Terminations (T1+T2, Figure 2e–h). The stack counts (Figure 2d,h) show that the two versions differ mainly in the younger half, they are identical beyond 85 kyr BP. The latitudinal ranges in the young half are slightly smaller for the compilations T1+T2 than when all cores are compiled, but the mean latitudes of all cores are throughout the covered time window of the last 160 kyr in all cases (for both species and for both compilations) close to the equator (Figure 2d,g). This consistency in the mean latitude suggests that the incoming light which varied in its annual mean values between $\sim$420 W m^{-2} at the equator and $\sim$330 W m^{-2} around latitudes of 40° (Laskar et al., 2004) should only marginally affect the isotopic fractionation (e.g. Spero et al., 1991).

2.2 Benthic δ^{13}C

Focus of this study is the δ^{13}C of the surface ocean. However, for a rough comparison of δ^{13}C changes in the deep ocean we rely on the published δ^{13}C stack constructed from six deep Pacific core as contained in Lisiecki (2014). The six cores are all ODP cores (677, 846, 849, 1123, 1143, 1208) from between 2700 and 3500 m water depth, located between 42°S and 36°N. The deep Pacific δ^{13}C stack should cover the most depleted end member of the marine δ^{13}C cycle (Figure 3d) and should give some indication how δ^{13}C in deep ocean is performing in our simulations. More details on the stack are found in Lisiecki (2014).

2.3 The carbon cycle model BICYCLE-SE

2.3.1 Brief model description

At the core of BICYCLE — the Box model of the Isotopic Carbon cYCLE — sits an ocean (O) with 10 boxes and a terrestrial biosphere consisting of seven boxes (B) together with a one box atmosphere (A), in which the concentration of carbon (as DIC in the ocean, as pCO_2 in the atmosphere, as organic carbon in the biosphere) and both of the isotopes δ^{13}C and Δ^{14}C are traced (Köhler et al., 2005). Furthermore, in the ocean alkalinity, PO_4^{3-} as macro-nutrient and O_2 is represented. From the two variables of the marine carbonate system (DIC and alkalinity) all other variables (CO_2, HCO_3^-, CO_3^{2-} and pH) are calculated according to Zeebe and Wolf-Gladrow (2001) with updates of the dissociation constants pK_1 and pK_2 (Mojica Prieto and Millero, 2002). The ten ocean boxes distinguish 100 m deep equatorial (or wider tropical) surface waters in Atlantic and Indo-Pacific from 1000 m deep surface ocean boxes in the high latitudes (North Atlantic, Southern Ocean, North Pacific). In the model, wider tropical boxes range from 40°S to 40°N in the Indo-Pacific and to 50°N in the Atlantic, rather similar to the latitudinal coverage of the sediment cores from which $\Delta(\delta^{13}C_{rub})$ and $\Delta(\delta^{13}C_{sac})$ have been constructed. Deep ocean boxes represent all waters below 1 km in the three basin Atlantic, Southern Ocean, Indo-Pacific. In the equatorial regions the waters

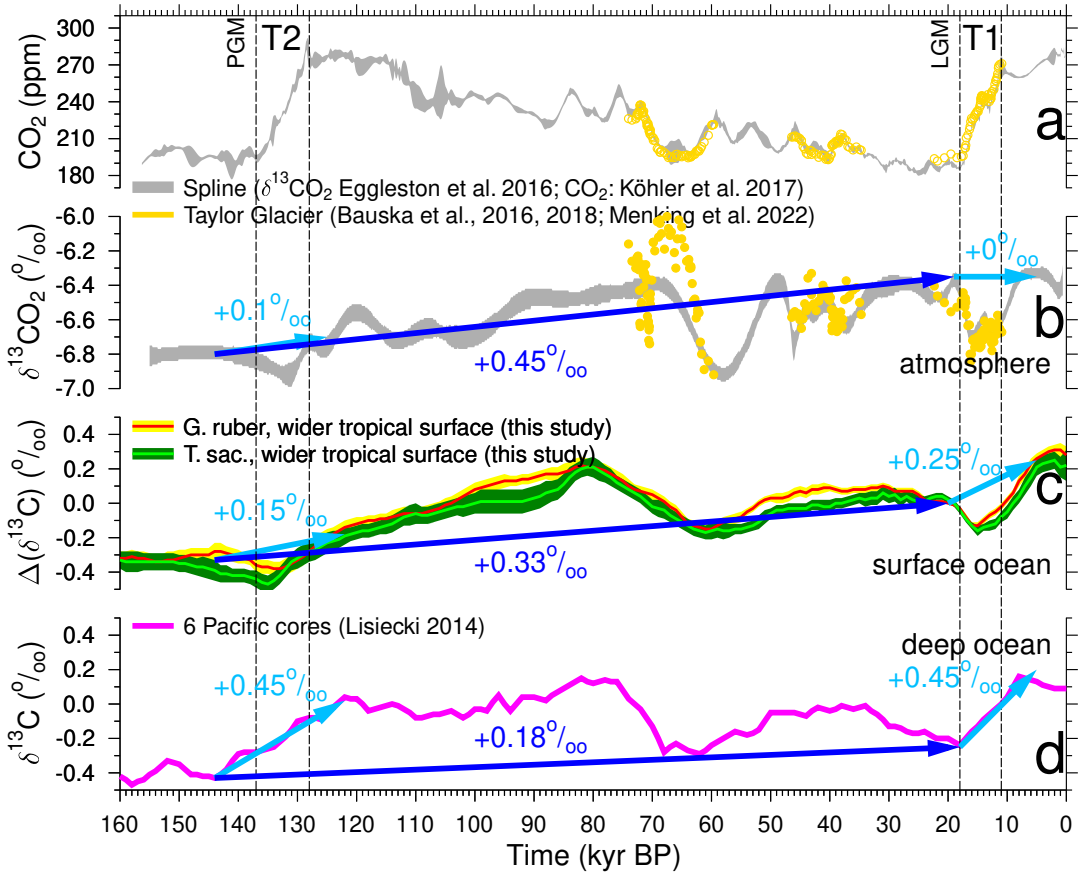

Figure 3. Carbon cycle time series of the last 160 kyr, including the Penultimate and Last Glacial Maximum (PGM, LGM) and Terminations 1 and 2 (T1, T2). Spline of atmospheric CO_2 (a) and $\delta^{13}CO_2$ (b) based on data from various ice cores (grey, $\pm 1\sigma$ around the mean, (Köhler et al., 2017a; Eggleston et al., 2016a)) and highly resolved recent data from the "horizontal ice core" approach in Taylor Glacier (yellow, (Bauska et al., 2016, 2018; Menking et al., 2022b)). (c) $\Delta(\delta^{13}C_{rub})$ and $\Delta(\delta^{13}C_{sac})$ averaging signals in the wider tropical surface ocean (this study, largely based on Mulitza et al., 2022). (d) Deep ocean $\delta^{13}C$ from benthic foraminifera stacked from six Pacific cores (Lisiecki, 2014).

between 100 and 1000 m water depth are described by intermediate boxes. The terrestrial biosphere (Köhler and Fischer, 2004) distinguishes C_3 and C_4 photosynthesis of grasses and trees, and soil carbon with different turnover times of up to 1000 years.

The model extension towards the version BICYCLE-SE used here, that can take care of solid Earth processes, is sketched in Figure 4. The main improvement documented in detail in Köhler and Munhoven (2020) is the implementation of a sediment module, that captures early diagenesis in a 8 cm deep sedimentary mixed layer (M), under which numerous historical layers are implemented. In effect, we now simulate the subsystem of the global carbon cycle consisting of atmopshere, ocean, terrestrial biosphere and sedimentary mixed layer (AOBM) within BICYLE-SE. In each of the three ocean basins (Atlantic; Southern

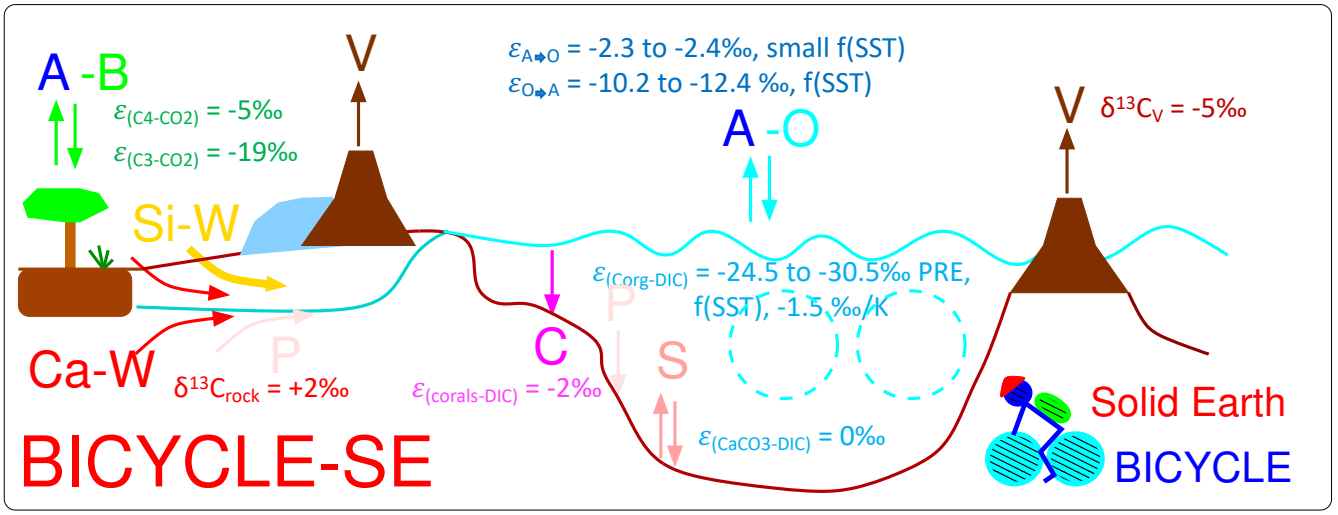

Figure 4. Sketch of the Box model of the isotopic carbon cycle, version solid Earth (BICYCLE-SE), modified from Köhler and Munhoven (2020). V: outgassing of CO_2 from volcanoes on land potentially and temporally overlain by land ice and from hot spot island volcanoes (and mid ocean ridges, not shown) influenced by changing sea level; C: shallow water carbonate deposition due to coral reef growth; Si-W: silicate weathering and Ca-W: carbonate weathering with different sources of C, but both delivering HCO_3^--ions into the ocean; P: PO_4^{3-} riverine input and sedimentary burial; S: $CaCO_3$ sedimentation and dissolution. A-B: atmosphere-biosphere exchange of CO_2; A-O: atmosphere-ocean exchange of CO_2. The cyan-coloured broken circles mimic the two overturning cell in the Atlantic and Indo-Pacific Ocean. The isotopic fractionation ε during exchange processes, or the prescribed $\delta^{13}C$ of external fluxes are given, summarising the parametrisation of the ^{13}C cycle within the model.

Ocean, Indo-Pacific) the pressure-dependent carbonate system is calculated for every 100 m water depth and depending on the over- or undersaturation of the carbonate-ion concentration $CaCO_3$ is either accumulated or dissolved. Parametrisation and realisation of the sedimentary processes directly follows Munhoven and François (1996) and Munhoven (1997). The carbon isotopes in the sedimentary mixed layer are only followed in aggregated boxes (one for each of the three ocean basin).

Equipping BICYCLE with a process-based sediment module enables the revised model version BICYCLE-SE to address questions related to changes in solid Earth carbon fluxes in detail and on long-term. Roughly speaking the following processes are considered: 1) CO_2 outgassing from volcanoes on land, hot spot island volcanoes and mid ocean ridge (MOR) hydrothermal activity is realised as partly being dependent on changing sea level. 2) Coral reef growth is a known shallow water carbonate sink, that is to some extent also following sea level rise. 3) Weathering of silicate or carbonate rocks on land, consuming different amounts of atmospheric CO_2, and both leading to bicarbonate fluxes into the ocean. These solid Earth processes are not directly coupled to each other. Their implementation into the model might therefore lead to temporal offsets in various variables, to which the sediment module might react in a carbonate compensation feedback. Further details on the model and the time-dependent forcing are found in Köhler and Munhoven (2020). Part of this brief model description has been taken from Köhler (2020).

2.3.2 Complete formulation of the ^{13}C cycle in BICYCLE-SE

The following isotopic fractionations are now considered in the BICYCLE-SE model. For this study the whole δ^{13}C cycle has been revised. While isotopic fractionations are given here in the $\varepsilon_{(\mathrm{A-B})}$-notation (in ‰) they are implemented after Zeebe and Wolf-Gladrow (2001) in the model as fractionation factors $\alpha_{(\mathrm{A-B})}$. Both are related after

$$\varepsilon_{(\mathrm{A-B})} = 1000 \cdot (\alpha_{(\mathrm{A-B})} - 1). \quad (1)$$

Furthermore, $\alpha_{(\mathrm{A-B})}$ is related to δ^{13}C in reservoirs A and B after

$$\alpha_{(\mathrm{A-B})} = \frac{\delta^{13}\mathrm{C_A} + 1000}{\delta^{13}\mathrm{C_B} + 1000}. \quad (2)$$

There is no convention if the initial or final reservoir is given as A or B here, however here A is always the final and B the initial reservoir of the fractionation process. In some cases a specific process instead of two reservoirs is mentioned in the subscript, e.g. $\varepsilon_{(\mathrm{a\to o})}$ and $\varepsilon_{(\mathrm{o\to a})}$ for the atmosphere-ocean gas exchange, for which not only the two different reservoirs, but also the direction of the flux plays a role for the size of the isotopic fractionation. In that case the quantified fractionation implies an isotopic depletion connected with the related process for $\varepsilon < 0$‰.

Air-sea gas exchange: Using the measurements from Zhang et al. (1995) we formulate, following in most parts Marchal et al. (1998), for the isotopic fractionation during gas exchange to be consisting of contributions from equilibrium (α^{eq}) and kinetic (α^{k}) fractionation ($\alpha^{\mathrm{total}} = \alpha^{\mathrm{eq}} \cdot \alpha^{\mathrm{k}}$). For the atmosphere-to-ocean CO_2 flux a temperature-dependent equilibrium fractionation of $\varepsilon^{\mathrm{eq}}_{\mathrm{a\to o}} = \varepsilon^{\mathrm{eq}}_{(\mathrm{aq-g})} = -1.31 + 0.0049 \cdot \mathrm{T_C}$ between dissolved (aq) and gaseous (g) CO_2 and a $\varepsilon^{\mathrm{k}}_{\mathrm{a\to o}} = -1.08$‰ is used. Note, $\varepsilon^{\mathrm{k}}_{\mathrm{a\to o}}$ differs by –0.2‰ from $\varepsilon^{\mathrm{k}}_{\mathrm{o\to a}} = -0.88$‰ for the ocean-to-atmosphere flux, a necessary correction already given in Zhang et al. (1995), but to our knowledge only rarely applied. For the reverse ocean-to-atmosphere flux we use the equilibrium fractionation $\alpha^{\mathrm{eq}}_{\mathrm{o\to a}} = \alpha^{\mathrm{eq}}_{(\mathrm{aq-DIC})} = \sum_i f_i \alpha_{(\mathrm{aq-i})}$ with f_{i} being the relative shares of CO_2, HCO_3^- and CO_3^{2-} on DIC in the representative ocean box. Furthermore, from the available measurements in Zhang et al. (1995) we derive: $\alpha_{(\mathrm{aq-HCO_3^-})} = \frac{\alpha_{(\mathrm{aq-g})}}{\alpha_{(\mathrm{HCO_3^- -g})}}$, $\alpha_{(\mathrm{aq-CO_3^{2-}})} = \frac{\alpha_{(\mathrm{aq-g})}}{\alpha_{(\mathrm{CO_3^{2-} -g})}}$ and $\alpha_{(\mathrm{aq-CO_2})} = 1$ using $\varepsilon_{(\mathrm{CO_3^{2-} -g})} = 7.22 - 0.052 \cdot \mathrm{T_C}$ and $\varepsilon_{(\mathrm{HCO_3^- -g})} = 10.78 - 0.114 \cdot \mathrm{T_C}$ with $\mathrm{T_C}$ being the sea surface temperature in °C.

Marine biology: The preindustrial marine export production of organic carbon at 100 m water depth is set to 10 PgC/yr (which in the model can increase in glacial periods due to iron fertilisation in the Southern Ocean up to 13 PgC/yr, Figure S1d) with a fixed molar rain ratio of organic C:$CaCO_3$ of 10:1. Existing data on fractionation during marine organic matter production (marine photosynthesis) are rather weak in determining if and how it depends on CO_2 (Young et al., 2013; Brandenburg et al., 2022; Liu et al., 2022). Furthermore, as discussed in Brandenburg et al. (2022) some species might contain so-called carbon concentrating mechanisms and use not CO_2, but HCO_3^- as source of their carbon, in which case a completely different isotopic fractionation during marine photosynthesis ($\varepsilon_{(\mathrm{C_{org}-DIC})}$) would follow. We base our initial formulation of $\varepsilon_{(\mathrm{C_{org}-DIC})}$ on the data compilation of $\delta^{13}\mathrm{C_{POC}}$ in Verwega et al. (2021) who found

a dependency on latitude. Using average preindustrial $\delta^{13}C_{DIC}$ of +2.5‰ (Schmittner et al., 2013) as starting values and the $\delta^{13}C_{POC}$ in Verwega et al. (2021) of –22, –24, –28‰ for low, high northern, and high southern latitudes, respectively, and approximating $\varepsilon_{(C_{org}-DIC)} \approx \delta^{13}C_{POC}$ - $\delta^{13}C_{DIC}$, we come up with the following isotopic fractionation $\varepsilon_{(C_{org}-DIC)}$ of $-24.5, -26.5$, and -30.5‰ accordingly. This approximation is motivated by the high uncertainties in $\delta^{13}C_{POC}$ as documented in Verwega et al. (2021).

The spread in $\delta^{13}C_{POC}$ in the data of Verwega et al. (2021) is huge, ranging from -15 to -35‰. Furthermore, they confirmed the finding of earlier studies (Young et al., 2013; Lorrain et al., 2020) that $\delta^{13}C_{POC}$ becomes much more depleted over time than what is explainable by the ^{13}C Suess effect (Keeling, 1979). In details, between 1960 and 2010 $\delta^{13}C_{POC}$ decreased by about 3 ± 4‰. The Suess Effect shows a decrease in atmospheric $\delta^{13}CO_2$ of about 1.5‰ during that time (Rubino et al., 2013) and it is known that in the ocean the Suess Effect is decreasing with depth (Eide et al., 2017). At the same time, global mean temperature rose by about 0.8 K (Rohde and Hausfather, 2020). This shift in $\delta^{13}C_{POC}$ is probably caused by a shift in the composition of the phytoplankton communities. We therefore use the values derived in the previous paragraph from Verwega et al. (2021) as our preindustrial parameter values of $\varepsilon_{(C_{org}-DIC)}$ to which we add a temperature-dependent part of -1.5‰ for any K the sea surface temperature in the relevant surface ocean box disagrees from its preindustrial value. The assumed value fits in the range of recent temperature-dependent $\delta^{13}C_{POC}$ found in Verwega et al. (2021) and has been obtained by tuning to simulate $\delta^{13}CO_2$ at preindustrial times to be similar to its values at LGM, as seen in the ice core data (Figure 3b). This leads to $\varepsilon_{(C_{org}-DIC)}$ at LGM of $-19.3, -20.4, -24.4$‰ for low, high northern, or high southern latitudes, respectively.

Data are also rather uncertain for the isotopic fractionation during the formation of $CaCO_3$. We assume, in agreement with Buitenhuis et al. (2019), that 65% of the $CaCO_3$ exported in the abyss consists of aragonite and 35% of calcite. Calcite is either produced by coccolithophores or planktic foraminifera. Some coccolithophore species suggest an enrichment, others a depletion in $\delta^{13}C$ in their shells with respect to $\delta^{13}C_{DIC}$ in the surrounding water (Ziveri et al., 2003). For planktic foraminifera the CIE is one of various possible processes of isotopic fractionation hypothesised to occur during hard shell formation (Bijma et al., 1999; Zeebe et al., 2008; Kimoto, 2015). Isotopic fractionation factors are in comparison to $\varepsilon_{(C_{org}-DIC)}$ rather small and in the case of the CIE species-specific (Spero et al., 1999). We therefore choose in the model to set the fractionation during calcite production to be neutral with respect to ^{13}C, thus $\varepsilon_{(cal-DIC)} = 0$‰, but we will consider the CIE in post-processing when comparing simulations with reconstructions. For simplicity and due to missing further evidence for fractionation during aragonite production $\varepsilon_{(ara-DIC)}$ was also kept at 0‰. More general, we keep $\varepsilon_{(CaCO_3-DIC)} = 0$‰.

The shallow water sink of carbonate in corals is assumed to have a $\delta^{13}C$ that follows after an isotopic fraction of $\varepsilon_{(corals-DIC)} = -2$‰ from the $\delta^{13}C$ of the DIC in the surface waters. This value is based on a combination of recent data, paleo data from the Great Barrier reef and insights from simulations (Linsley et al., 2019; Felis et al., 2022).

Terrestrial biosphere: On land, isotopic fractionation is only assumed to occur during photosynthesis with $\varepsilon_{(C_3-CO_2)} = -19‰$ and $\varepsilon_{(C_4-CO_2)} = -5‰$ for C_3 (all woody plants and some grasses) and C_4 (some other grasses) photosynthesis, respectively (Vogel, 1993; Lloyd and Farquhar, 1994).

External fluxes to the AOBM subsystem: The volcanic CO_2 outgassing flux is assumed to have a fixed $\delta^{13}C$ signature ($\delta^{13}C_V$) of $-5.0‰$, the typical mean value for volcanic outgassing (e.g. Deines, 2002; Roth and Joos, 2012), but note that the uncertainty is $\pm 3‰$.

From the two weathering fluxes based on either silicate or carbonate rocks, only the latter has a contribution which bring new carbon into the system. Here, 50% of the carbon that as bicarbonate — the weathering product — is entering the ocean with a $\delta^{13}C$ signature ($\delta^{13}C_{rock}$) of +2‰ — identical to the most likely $\delta^{13}C$ values in carbonate rocks build during the Phanerozoic (Bachan et al., 2017). The carbon for the other half of the carbonate weathering flux and for all of the silicate weathering flux is assumed to come from CO_2 in the soil environment. We therefore assume that this CO_2 might be dominated by soil respiration fluxes and therefore a $\delta^{13}C$ signature that corresponds to the mean value of the two soil carbon boxes is assumed here.

To balance the inflow of ^{13}C via volcanism and weathering the model has been tuned for long-term stable mean $\delta^{13}C$ values in the AOBM subsystem by the following sink: About 6% of the organic carbon, that is exported from the surface boxes into the abyss is assumed to be lost in the sediment. Note, that this number has been tuned with the previous version of the ^{13}C cycle in operation (Köhler and Munhoven, 2020), but has not been revised thereafter.

2.3.3 Simulation Setup and Scenarios

The BICYCLE-SE model simulates the global carbon cycle as function of changing time-dependent physical boundary conditions (forcing), which are nearly identical to the simulations published in Köhler and Munhoven (2020) and which are also in detail described in that study. Briefly, ocean circulation is prescribed from modern data of the WOCE experiment, while its main temporal changes are restricted to: (a) the AMOC, which is reduced from modern/interglacial 16 Sv to 10 Sv during glacial periods (Figure S1b); (b) Southern Ocean (SO) vertical deep mixing is a function of SO sea surface temperature (Figure S1c). Ocean and land temperature are prescribed from reconstructions (Figure S1e), ocean salinity is varied as function of prescribed sea level (Figure S1a). Additionally, aeolian iron input in the SO is assumed to follow dust fluxes measured in Antarctic ice cores, which might change marine biology in the SO from an iron-limited to an iron-unlimited regime, increasing glacial export production of organic matter to the deep ocean (Figure S1d). The standard scenario SEi used here is — apart from the revised $\delta^{13}C$ cycle — nearly identical to the scenario SE in Köhler and Munhoven (2020). The only difference is that in the application here we revised the applied equatorial sea surface temperature (SST). It has been based in previous applications on changes in planktic $\delta^{18}O$ in only one ODP record. Now we use the SST stack from Barth et al. (2018), which is based on a compilation of SST from 15 non-polar sediment cores. This leads to only minor changes in atmospheric CO_2 of less than 5 ppm, but is important for the ^{13}C cycle, and its temperature-dependencies (isotopic fractionation during atmosphere-ocean gas exchange and during carbon uptake by the marine biology). Simulations are started from interglacial conditions around 210

Table 1. Overview of simulation scenarios.

Name	Description
SEi	standard run for BICYCLE-SE with updated ^{13}C cycle
SEi0	as SEi, but without temperature-dependent contribution to $\varepsilon_{(\mathrm{C_{org}-DIC})}$
C1	as SEi, but atmospheric $\delta^{13}CO_2$ is prescribed from data (Eggleston et al., 2016a)
C1CO2	as SEi, but atmospheric records ($\delta^{13}CO_2$, CO_2) are prescribed from data (Eggleston et al., 2016a; Köhler et al., 2017a)

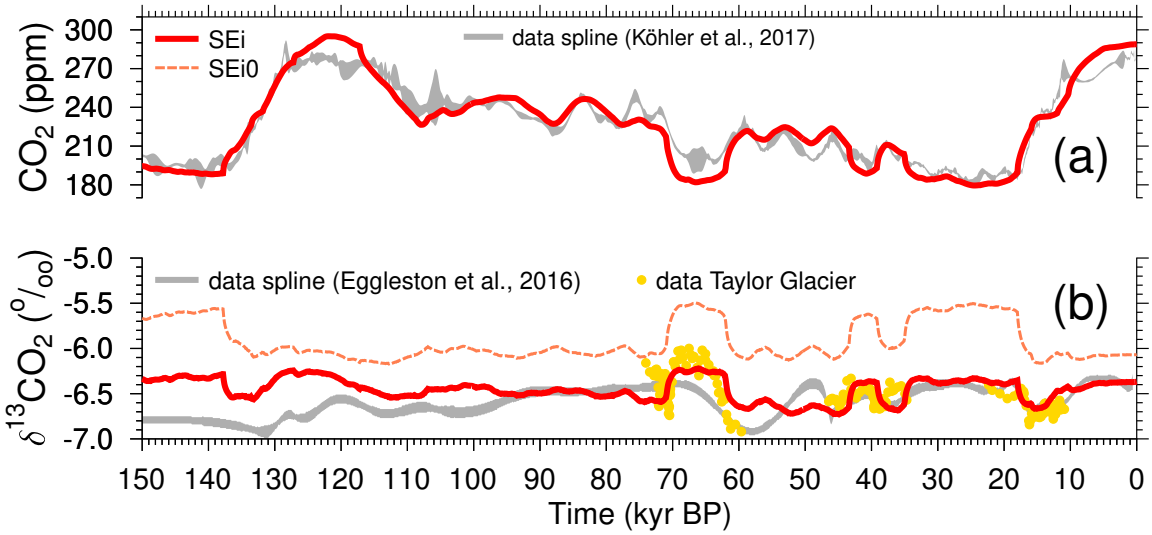

Figure 5. Simulation results and comparison to data splines for (a) atmospheric CO_2, and (b) atmospheric $\delta^{13}CO_2$. Results for scenario SEi (standard) and SEi0 are shown. The latter differs from the standard run by a lack of temperature-dependency in $\varepsilon_{(\mathrm{C_{org}-DIC})}$.

kyr BP. Scenario SEi0 is only performed to illustrate how the implementation of the temperature-dependency in $\varepsilon_{(\mathrm{C_{org}-DIC})}$ improve the simulated ^{13}C cycle, illustrated by plotting atmospheric $\delta^{13}CO_2$ against data in Figure 5b.

Simulated changes in the atmospheric record are already in scenario SEi not too far away from the reconstructions, especially in CO_2 (Figure 5a). However, to bring the carbon cycle in atmosphere and surface ocean as close as possible to the reconstructions we perform additional simulations in which the atmospheric $\delta^{13}CO_2$ alone (scenario C1) or together with atmospheric CO_2 (scenario C1CO2) is forced by the reconstructions. Here, we use the data splines as plotted in Figure 3a,b (Eggleston et al., 2016a; Köhler et al., 2017a) and ignore the higher resolved data from Taylor Glacier since these more abrupt changes in $\delta^{13}CO_2$ are either during the last 50 kyr to a large extent covered in the dynamics of the spline (Bauska et al., 2016, 2018) or around 70 kyr BP (Menking et al., 2022b) probably not recorded in our marine sediment records. This implies that internally calculated fluxes are overwritten by changes that are necessary to keep the simulated atmospheric carbon variables identical to the reconstructions. This approach is typically applied in CO_2 concentration-driven present day or future ocean carbon cycle

simulations (e.g. Hauck et al., 2020). It has already been used in BICYCLE-SE for ^{14}C to obtain radiocarbon in the surface ocean as close to the data as possible during the construction of the most recent marine radiocarbon calibration curve Marine20 (Heaton et al., 2020) and subsequent studies (Köhler et al., 2022). However, since atmospheric CO_2 and $\delta^{13}CO_2$ are normally prognostic variables of the model and their calculated changes should be derived out of the model's differential equations followed by a proper integration scheme, this approach slightly violates the mass conservation. It nevertheless guarantees that simulated surface ocean variables of the carbon cycle are within the model realm as consistent as possible with the atmospheric reconstructions. An overview of the applied simulation scenarios is compiled in Table 1.

2.4 Data analysis

Linear regression was performed with the software MATLAB (The MathWorks Inc., 2023). The uncertainties of the fits are approximated by root-mean-square-errors calculated after $s = \sqrt{\frac{1}{n}\sum_{i=1}^{n}(y_i - f_i)^2}$, with f_i being the calculated values according to the linear regression equations. In cases in which the uncertainties in both variables should be considered we used the function "linfitxy", version 1.2.0.0 (Browaeys, 2023). The frequency analysis was performed using R (R Core Team, 2023), including the function "coh" from the R-package seewave, version 2.2.3, calculating coherence.

3 Results and Discussion

3.1 Overview on ^{13}C cycle changes over the last 160 kyr

Reconstructed changes in the late Quaternary carbon cycle are still not completely understood. The ice cores give us a precise picture of atmospheric CO_2 (Bereiter et al., 2015; Köhler et al., 2017a) (Figure 3a), which in the meantime has also been met reasonably well with various different carbon cycle models (e.g. Menviel et al., 2012; Ganopolski and Brovkin, 2017; Khatiwala et al., 2019; Köhler and Munhoven, 2020). These findings suggest, that the main processes responsible for the observed changes on orbital timescales might indeed have been identified, although results are to some extent model-dependent and improvements in details are certainly necessary.

The corresponding atmospheric $\delta^{13}CO_2$, now available over the last 155 kyr (Eggleston et al., 2016a), however, is in all its features still waiting for a process-based interpretation (Figure 3b). Since $\delta^{13}CO_2$ helps to pinpoint on processes responsible for CO_2 changes, any simulation that is able to explain one without the other might need to be interpreted with caution. Models suggest that especially physical and biological processes in the Southern Ocean processes robustly influence $\delta^{13}CO_2$, while the impact of the Atlantic meridional overturning circulation (AMOC) on $\delta^{13}CO_2$ seems to be model-dependent (Menviel et al., 2015). Consequently, the abrupt drop in $\delta^{13}CO_2$ at the onset of Termination 1 (T1) (Smith et al., 1999; Schmitt et al., 2012) is nowadays understood to be caused by marine processes, while subsequent $\delta^{13}CO_2$ changes during T1 and its recovery during the Holocene to LGM-like values were potentially related to a mixture of oceanic and terrestrial processes (Köhler et al., 2005; Bauska et al., 2016).

Two largely unexplained features stand out in the 155 kyr $\delta^{13}CO_2$ record. First, there exist a long-term trend by +0.45‰ from the Penultimate and the Last Glacial Maximum (PGM and LGM). When first discovered (Schneider et al., 2013) it has been hypothesised that changes in the isotopic composition of solid Earth fluxes or of their intensities or long-term peat build-up might be responsible for them. Second, a 0.5‰ deep and nearly 20 kyr long minima centred around 58 kyr BP happened, rather uncorrelated with CO_2 changes. Eggleston et al. (2016a) hypothesise that the $\delta^{13}CO_2$ minima might have been partially caused by a change in ocean stratification between Marine Isotope Stage (MIS) 4 and MIS 3, allowing for a different amount of isotopically light carbon being stored in the deep ocean. Recently, high resolution data of $\delta^{13}CO_2$ from Taylor Glacier covering 74 to 59.5 kyr BP including MIS 4 and the drop into the $\delta^{13}CO_2$ minimum have been published (Menking et al., 2022b) showing more variability and between 66 and 60 kyr BP with –1‰ a twice as large change as previously contained in the smoothed record of Eggleston et al. (2016a). Menking et al. (2022b) also performed first model simulations in order to understand which processes might be responsible for the reconstructed changes in the carbon cycle. However, to our knowledge none of the ideas put forward in Schneider et al. (2013) for the long-term trend in $\delta^{13}CO_2$ have so far been convincingly and successfully verified with carbon cycle model simulation. Furthermore, 400–500 kyr variability in $\delta^{13}C$ related to slow eccentricity changes found throughout the Cenozoic (e.g. Pälike et al., 2006; Russon et al., 2010; Ma et al., 2011; Wang et al., 2014; Paillard, 2017) might be superimposed on faster variations, making a process-based understanding of observed changes in $\delta^{13}CO_2$ even more challenging.

Sediment cores covering the Anthropocene clearly show that the $\delta^{13}C$ of *G. ruber* and *T. sacculifer* shells ($\delta^{13}C_{\mathrm{rub}}$, $\delta^{13}C_{\mathrm{sac}}$) faithfully reflects changes in $\delta^{13}C_{\mathrm{DIC}}$ caused by the $\delta^{13}C$ Suess Effect (Al-Rousan et al., 2004; Black et al., 2011), albeit with a notable offset. This offset might be influenced by the CIE (e.g. Spero et al., 1997), light intensity (e.g. Spero et al., 1991) and the size of the foraminiferal shells (e.g. Oppo and Fairbanks, 1989). Our new mono-specific stacks from the wider tropical surface ocean of $\Delta(\delta^{13}C_{\mathrm{rub}})$ and $\Delta(\delta^{13}C_{\mathrm{sac}})$ (Figure 3c) contain a G/IG rise of 0.25‰ across T1, but of only 0.15‰ across T2, while atmospheric $\delta^{13}CO_2$ at the same time rose by 0.1‰ (T2), or stayed constant (T1) (Figure 3b), showing local minima during terminations in both records. Deep ocean benthic $\delta^{13}C$ (Figure 3d) is here approximated by a stack from six deep Pacific cores (Lisiecki, 2014), that contains a G/IG rise of 0.45‰ across both T1 and T2. This value is on the upper end of the 95% confidence interval of compilations of marine $\delta^{13}C$ changes across T1 (Peterson et al., 2014; Peterson and Lisiecki, 2018) which suggest to represent global ocean wide changes. The marine time series, both from surface and deep ocean, also contain wide and deep minima around 60 kyr BP, similarly to the smoothed atmospheric $\delta^{13}CO_2$ data of Eggleston et al. (2016a), but different to the higher resolved Taylor Glacier $\delta^{13}CO_2$ of Menking et al. (2022b). Furthermore, all marine $\delta^{13}C$ data, similarly as the atmospheric $\delta^{13}CO_2$, contain a long-term rise from PGM to LGM (about +0.33‰ in the wider tropical surface ocean, +0.18‰ in the deep Pacific, Figure 3), which might be potentially connected with the 400-to-500 kyr variability.

Before we start with deeper model-based interpretation of the ^{13}C cycle, we have a closer look on our new isotope stacks. The size of the CIE as detected from laboratory experiments in both species differs by nearly a factor of two, -0.0089 and -0.0047 ‰ change in $\delta^{13}C$ per μmol kg^{-1} of [CO_3^{2-}] for *G. ruber* and *T. sacculifer*, respectively, and of -0.0022 and -0.0014 ‰ change in $\delta^{18}O$ per μmol kg^{-1} of [CO_3^{2-}] for *G. ruber* and *T. sacculifer*, respectively (Spero et al., 1999). Therefore, if the CIE plays a role for how the isotopes of the surface ocean are recorded in the foraminifera shells on orbital

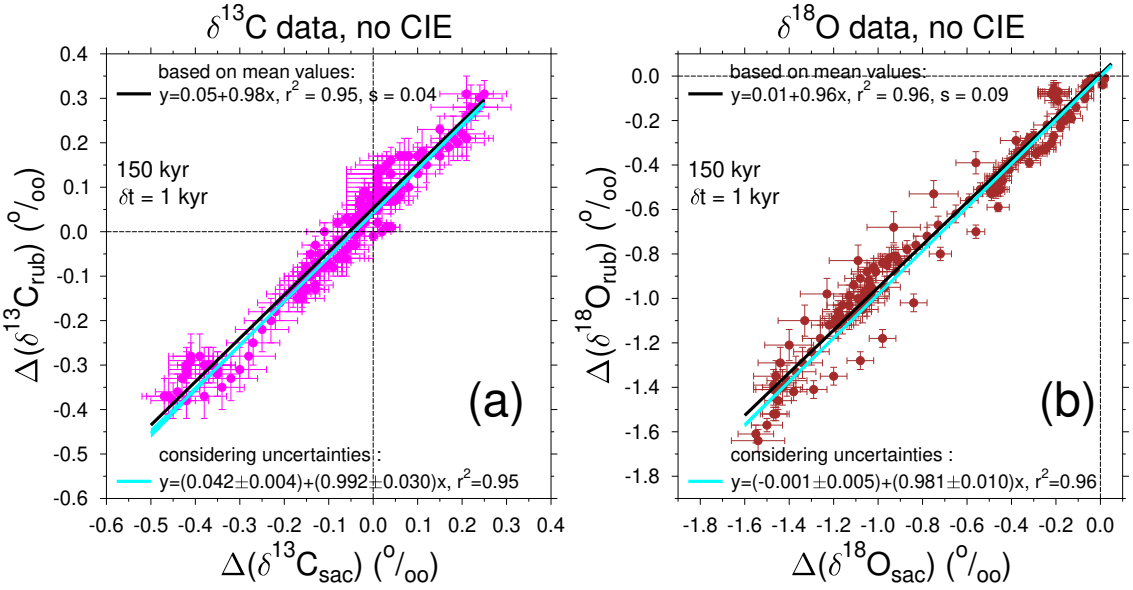

Figure 6. Scatter plot of our new stacks (a) $\Delta(\delta^{13}\mathrm{C_{rub}})$ versus $\Delta(\delta^{13}\mathrm{C_{sac}})$ and (b) $\Delta(\delta^{18}\mathrm{O_{rub}})$ versus $\Delta(\delta^{18}\mathrm{O_{sac}})$. Data stacks without corrections for the CIE are plotted. The time series are restricted to data of last 150 kyr to allow comparison later-on with simulation results which were based on the only 155 kyr long atmospheric $\delta^{13}CO_2$ record. Linear regressions using only the mean values and when using also uncertainties in both x and y are performed. The root-mean-square-error is depicted by s.

timescales then the two mono-specific time series in both δ^{13}C and δ^{18}O should differ. At first glance (Figure 2a,b) the time series are remarkable similar. A more quantitative evaluation is obtained by calculating the linear regression from scatter plots, when results based on one species are plotted against those of the other. Doing so (Figure 6) reveals for δ^{13}C that on average changes are identically recorded in both species. In other words, the linear slope of $\Delta(\delta^{13}\mathrm{C_{rub}})$ against $\Delta(\delta^{13}\mathrm{C_{sac}})$ is 0.98 ($r^2 = 0.95, s = 0.04‰$) or 0.99±0.03 ($r^2 = 0.95$) when considering the uncertainties of our stack during regression. For δ^{18}O the agreement is only slightly worse, the regression slope of $\delta^{18}\mathrm{O_{rub}}$ against $\delta^{18}\mathrm{O_{sac}}$ is 0.96 ($r^2 = 0.96, s = 0.09‰$) or 0.98±0.01 ($r^2 = 0.96$) with uncertainties. Since $\Delta(\delta^{13}\mathrm{C_{rub}})$ and $\Delta(\delta^{13}\mathrm{C_{sac}})$ are on average recording virtually the same changes it is difficult to image how the species-specific CIE can play a role here. Due to the small amplitudes of the CIE in δ^{18}O it is yet inconclusive if the CIE plays a role for $\Delta(\delta^{18}\mathrm{O_{rub}})$ versus $\Delta(\delta^{18}\mathrm{O_{sac}})$.

3.2 Simulated δ^{13}C cycle using the BICYCLE-SE model

General dynamics of the global carbon cycle in the BICYCLE-SE model have been analysed in detail in Köhler and Munhoven (2020). We here focus on the revised δ^{13}C cycle, but see how atmospheric CO_2 in scenario SEi meets the ice core data in Figure 5a. Note, that some analysis of δ^{13}C in the precursor model BICYCLE without solid Earth contributions have been

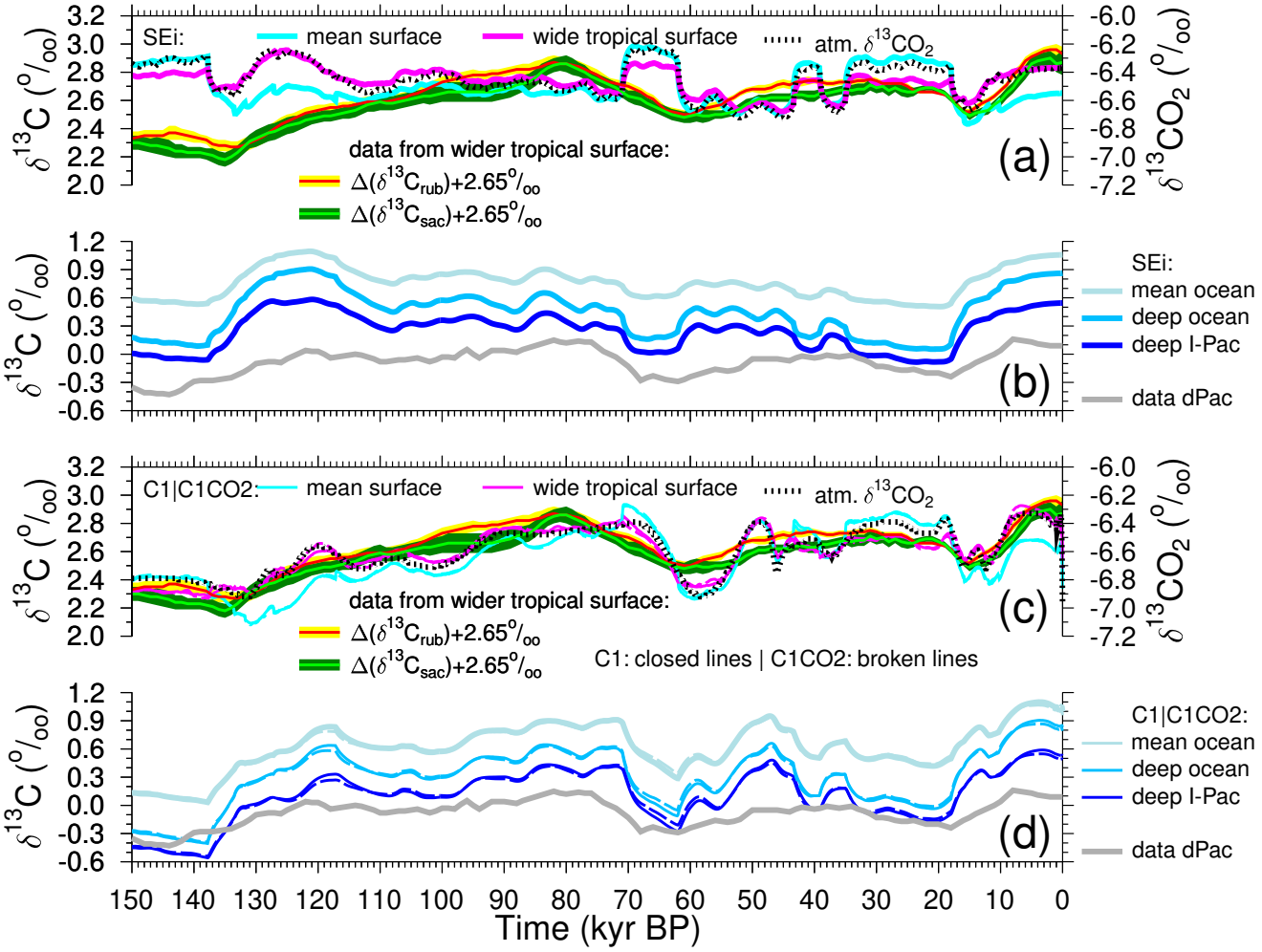

Figure 7. Simulated surface and deeper ocean δ^{13}C time series from scenario SEi (a, b) and scenarios C1 and C1CO2 (c, d) compared with reconstructions. (a,c) Simulated $\delta^{13}C_{DIC}$ in the global mean surface and in the wider tropical surface ocean together with simulated atmospheric $\delta^{13}CO_2$ (right y-axis) are plotted together with our new stacks from the wider tropical surface ocean, $\Delta(\delta^{13}C_{rub})$ and $\Delta(\delta^{13}C_{sac})$ shifted by +2.65‰ to meet simulated surface $\delta^{13}C_{DIC}$ at LGM. In (b,d) simulated $\delta^{13}C_{DIC}$ for the deep Indo-Pacific (I-Pac), the mean deep ocean and the mean global ocean are plotted together with δ^{13}C from benthic foraminifera stacked from six cores in the deep Pacific (dPac) (Lisiecki, 2014). In (c,d) the scenarios C1 (closed lines) and C1CO2 (broken lines) are plotted together. Most of the time the differences between both are so small that lines are indistinguishable.

described in Köhler et al. (2010), who showed that the model misses variations in δ^{13}C related to periodicities longer than 100-kyr.

Atmospheric $\delta^{13}CO_2$ (Eggleston et al., 2016a) is met by the results from scenario SEi only roughly, including some millennial-scale variations around 50–30 kyr BP and the transition from LGM to preindustrial, shows some deficit the sec-

ond half of T1 and in the Holocene (Figure 5b). The PGM-to-LGM trend of 0.45‰ and the minimum around 60 kyr BP are both largely unexplained in this simulation. The attribution of changes in $\delta^{13}CO_2$ to individual processes in the ocean and land carbon cycle has been done before for the precursor model BICYCLE (Köhler et al., 2005, 2010), and is not repeated here, since the misfit to the data indicates some fundamental shortcomings.

How simulated changes in atmospheric $\delta^{13}CO_2$ compare to simulated changes in various marine $\delta^{13}C_{DIC}$ time series is shown for scenario SEi in Figure 7a,b. Both global mean surface $\delta^{13}C_{DIC}$ and wider tropical surface $\delta^{13}C_{DIC}$ show clear similarities with atmospheric $\delta^{13}CO_2$. Here, surface values are area-weighted averages covering either the global ocean or the two equatorial ocean boxes in case of the wider tropics, which spatially cover a similar area as the sediment cores used for our new stacks $\Delta(\delta^{13}C_{rub})$ and $\Delta(\delta^{13}C_{sac})$. During glacial times and the onset of deglaciations the dynamics in global mean surface $\delta^{13}C_{DIC}$ (cyan line in Figure 7a) are in close agreement with $\delta^{13}CO_2$ in the atmosphere (black broken line in Figure 7a), while for the later part of the deglaciations and the interglacials the dynamics in wider tropical surface $\delta^{13}C_{DIC}$ (magenta line in Figure 7a) fits better to $\delta^{13}CO_2$ in the atmosphere. This difference is probably explained by the dynamics in the polar oceans. During glacial times, the Southern Ocean is highly stratified with little vertical exchange between surface and deep ocean. This stratification breaks down during the terminations and in interglacials allowing faster exchange of tracers between surface and deep ocean leading in the polar oceans to smaller surface-to-deep gradients in $\delta^{13}C_{DIC}$. In other words, the lower deep ocean $\delta^{13}C_{DIC}$ values have a larger impact on polar surface $\delta^{13}C_{DIC}$ during interglacials than during glacials leading to a divergence between $\delta^{13}C_{DIC}$ in the global mean surface and the wider tropical surface ocean. The scatter plots between atmospheric $\delta^{13}CO_2$ and either global mean surface or wider tropical surface ocean $\delta^{13}C_{DIC}$ show that the latter has the higher correlation (Figure S2, $r^2 = 0.82$ vs. $r^2 = 0.59$). Furthermore, frequency analysis showed that the coherence between atmospheric $\delta^{13}CO_2$ and wider tropical surface ocean $\delta^{13}C_{DIC}$ is in periodicities slower than 20 kyr higher than between atmospheric $\delta^{13}CO_2$ and global mean surface ocean $\delta^{13}C_{DIC}$ (Figure S3a). This implies, that simulations which agree in atmospheric $\delta^{13}CO_2$ with reconstructions (which will be achieved later-on in scenarios C1 and C1CO2) should contain a very likely realisation of $\delta^{13}C_{DIC}$ in the wider tropical surface ocean. A comparison of these simulated time series with our new mono-specific $\delta^{13}C$ stacks should therefore enable us to address if and how $\delta^{13}C$ has been modified during hard shell formation. For scenario SEi the misfit in simulated wider tropical surface ocean $\delta^{13}C_{DIC}$ and the new $\delta^{13}C$ reconstructions (Figure 7a) is large, but it is yet unclear if this discrepancy can be explained by the CIE or by other processes.

To understand how representative the reconstructed $\delta^{13}C$ stack from benthic foraminifera in six deep Pacific cores (Lisiecki, 2014) might be we compare it with various different simulated time series: $\delta^{13}C_{DIC}$ in the deep Indo-Pacific, in the mean deep ocean, or in the mean ocean (Figure 7b). Here, deep ocean results from the model refers to ocean boxes that contain waters deeper than 1 km. As expected the deep Indo-Pacific contains the end-member of the $\delta^{13}C$ cycle with the most depleted values. The mean deep ocean $\delta^{13}C_{DIC}$ is offset by 0.2–0.4‰ towards more positive values and shows larger G/IG amplitudes than $\delta^{13}C_{DIC}$ in the deep Indo-Pacific. The mean ocean is again 0.2–0.4‰ more positive in $\delta^{13}C_{DIC}$ than the mean deep ocean with again smaller G/IG amplitudes of 0.53‰ across T1. This number compares $\delta^{13}C_{DIC}$ in the last 6 ka with the mean at the LGM (23–19 ky BP) similarly as in Peterson et al. (2014) who proposed a mean ocean rise in $\delta^{13}C$ by 0.34 ± 0.19‰. However, be aware that in Peterson et al. (2014) the CIE in benthic foraminifera as deduced in Schmittner et al. (2017) is not included.

This suggests that the reconstructions are potentially recording a smaller G/IG change in δ^{13}C than how $\delta^{13}C_{DIC}$ in the deep ocean might have changed.

When discussing results of scenario SEi (Figure 7a) we have shown that once changes in the atmospheric $\delta^{13}CO_2$ are met by the simulations the model then also should give a reasonable answer for how $\delta^{13}C_{DIC}$ in the wider tropical surface ocean might have looked like. Furthermore, the close agreement of simulated and reconstructed atmospheric CO_2 (Figure 5a) suggests that the assumed carbon cycle changes in our approach might be one possible realisation that is not too far away from the real world changes. However, the misfit between simulation results from scenario SEi and reconstruction in the δ^{13}C cycle — linear regressions between simulations and reconstructions found no correlation at all ($r^2 \leq 0.02$, Figure S4a,b) — is not easily fixed. To improve our results we force in the following the model with the atmospheric records (scenario C1: only using $\delta^{13}CO_2$; scenario C1CO2: using both $\delta^{13}CO_2$ and CO_2) to have conditions in the surface ocean as close to reconstructions as possible. Doing so leads to even tighter correlations between simulated atmospheric $\delta^{13}CO_2$ and simulated $\delta^{13}C_{DIC}$ in the surface ocean than what we obtained for scenario SEi, the r^2-correlations between these variables are in scenarios C1 and C1CO2 with prescribed atmospheric $\delta^{13}CO_2$ $\geq$0.77 and $\geq$0.88 for global mean surface $\delta^{13}C_{DIC}$ and wider tropical surface $\delta^{13}C_{DIC}$, respectively (Figure S2). Again, the coherence is higher between atmospheric $\delta^{13}CO_2$ and the wider tropical surface ocean $\delta^{13}C_{DIC}$ than between atmospheric $\delta^{13}CO_2$ and the global mean surface ocean $\delta^{13}C_{DIC}$ (Figure S3b). Furthermore, in both scenarios the changes in simulated $\delta^{13}C_{DIC}$ in the wider tropical surface ocean agree remarkably well (r^2 between 0.76 and 0.78, Figure S4c–f) with changes in our new stacks $\Delta(\delta^{13}C_{rub})$ and $\Delta(\delta^{13}C_{sac})$ without consideration of the CIE (Figure 7c), at least on the orbital timescales. This effect is also seen by the rise in coherence between simulated wider tropical surface $\delta^{13}C_{DIC}$ and both our stacks from less than 0.1 (scenario SEi) to higher than 0.7 (scenario C1CO2) in the 41-kyr and 100-kyr bands (Figure S3c,d), while in the precession bands (19, 23-kyr) the coherence stayed below 0.6. Some more abrupt changes contained in the simulations are not recorded in the reconstructions, probably because bioturbation in the surface sediments together with the stacking procedure prevent our marine records from successfully resolving millennial-scale features. Thus, our forcing of atmospheric carbon records with data therefore seemed to be a promising approach to obtain simulated surface ocean in agreement with reconstructions for the slow frequency bands (41-kyr and beyond), while it seems to fail for precession and faster changes. When forcing atmospheric $\delta^{13}CO_2$ by data the temperature-dependent isotopic fractionation during marine photosynthesis in $\varepsilon_{(C_{org}-DIC)}$ is only of minor importance for the simulated surface ocean $\delta^{13}C_{DIC}$. If this effect is switched off the $\delta^{13}C_{DIC}$ in the wider tropical surface ocean differs in general by less than 0.05‰ from the values in scenario C1.

Furthermore, deep ocean $\delta^{13}C_{DIC}$ is on orbital time scale now also in better agreement with the data (Figure 7d), the r^2 of a linear regression between simulated deep Indo-Pacific $\delta^{13}C_{DIC}$ and reconstructed deep Pacific rises from 0.49 for scenario SEi to 0.77 and above for the scenarios forced by atmospheric carbon records (Figure S5), although the rise in mean ocean $\delta^{13}C_{DIC}$ during T1 has now been increased to 0.59‰. Considering a CIE of -2.6×10^{-3} ‰ per μmol kg^{-1} of [CO_3^{2-}] disturbance for epi-benthic foraminifera (Schmittner et al., 2017) simulated variations in deep ocean [CO_3^{2-}] of $+20$ μmol kg^{-1} (Köhler and Munhoven, 2020) would translate to a comparably small reduction in deep Pacific benthic δ^{13}C of up to 0.05‰. While the timing of changes in deep ocean [CO_3^{2-}] with highest values during the deglaciation is crucial to assess how such a benthic CIE would reduce the exisiting data/model mismatch a more thorough assessment of the benthic CIE would require

the comprehensive compilation of benthic δ^{13}C time series in different ocean basins, which is beyond the scope of this study. Note that the approximated amplitude of this benthic CIE is close to the measurement error of benthic δ^{13}C.

3.3 The importance of the carbonate ion effect for wider tropical surface ocean δ^{13}C

Although the initial analysis of our results when forced with atmospheric records already suggests only a minor, if any, role for the CIE in the interpretation of stacked mono-specific δ^{13}C on orbital timescales, in the following we make a more quantitative assessment. The CIE has not yet been implemented in the ^{13}C cycle of the model, but is only investigated here in post-processing. The carbonate ion concentration of either globally mean surface or wider tropical mean surface waters in our simulations are tightly anti-correlated to atmospheric CO_2 ($r^2 \geq 0.93$, Figure S6), which is a consequence of the marine carbonate system (Zeebe and Wolf-Gladrow, 2001). Both scenarios C1 and C1CO2 lead to rather similar results here, which suggests that the CO_2 forcing in scenario C1CO2 and its violation of mass conservation, is perturbing the carbon cycle only slightly. To be as close as possible to the reconstructions we nevertheless continue in the following by using results from scenario C1CO2, but results differ only slightly when based in scenario C1, thus our conclusions are independent from this choice.

Thus, CO_3^{2-} in wider tropical surface ocean in the simulation typically falls from maximum glacial values of $\sim$320 μmol kg^{-1} to interglacial minimum of $\sim$250 μmol kg^{-1} across both Terminations 1 and 2 (Figure 8a). This translates into a potential CIE of about 0.62‰ (Figure 8b) for *G. ruber* when we use the slope of $m = -0.0089$ ‰ per μmol kg^{-1} change in $[CO_3^{2-}]$, and of 0.33‰ for *T. sacculifer* (slope of $m = -0.0047$ ‰ per μmol kg^{-1} change in $[CO_3^{2-}]$ (Spero et al., 1999). The y-axis intercepts of the complete regressions for the CIE is determined in order to have maximum agreement between reconstructions and simulations during the LGM. When comparing the potential CIE to the simulated LGM-to-preindustrial (PRE) amplitude of only 0.16‰ in wider tropical surface waters (Figure 8c) the CIE-to-G/IG ratios are between a factor of 2 and 4 and CIE signals should clearly stand out in the paleo records. If we add this CIE to our simulated mean equatorial surface ocean $\delta^{13}C_{DIC}$ (Figure 8c) we end up with time series, which should compare well with the mono-species stacks of $\Delta(\delta^{13}C_{rub})$ and $\Delta(\delta^{13}C_{sac})$ (Figure 8d). However, this is not the case. The r^2 in the linear regressions between CIE-corrected $\delta^{13}C_{DIC}$ in wider tropical surface waters and reconstructions is reduced to 0.54 (*G. ruber*) and 0.68 (*T. sacculifer*), while it had been $\geq$0.76 without CIE correction (Figures S4, S7). When plotting results as hypothetically recorded in both species against each other we obtain a slope of 1.26 (Figure S8a). The slope between both time series without the CIE was $\sim$0.99 (Figure 6a). The consideration of the CIE did not lead to time series which agree better with each other. Thus, we conclude that both species *G. ruber* and *T. sacculifer* are already good recorders of changes in $\delta^{13}C_{DIC}$ in wider tropical surface ocean waters on orbital timescales.

3.4 Carbonate ion effect in δ^{18}O

The focus of this study is on stable carbon isotope δ^{13}C. However, during the construction of our mono-specific wider tropical stacks of $\Delta(\delta^{13}C_{rub})$ and $\Delta(\delta^{13}C_{sac})$ the corresponding stacks of $\Delta(\delta^{18}O_{rub})$ and $\Delta(\delta^{18}O_{sac})$ are easily-generated by-products initially used to cross-check the applied age models. However, these δ^{18}O data give us the possibility to also have a closer look on the role of the CIE in the recording of oxygen isotopes in foraminiferal shells. For that effort we need a

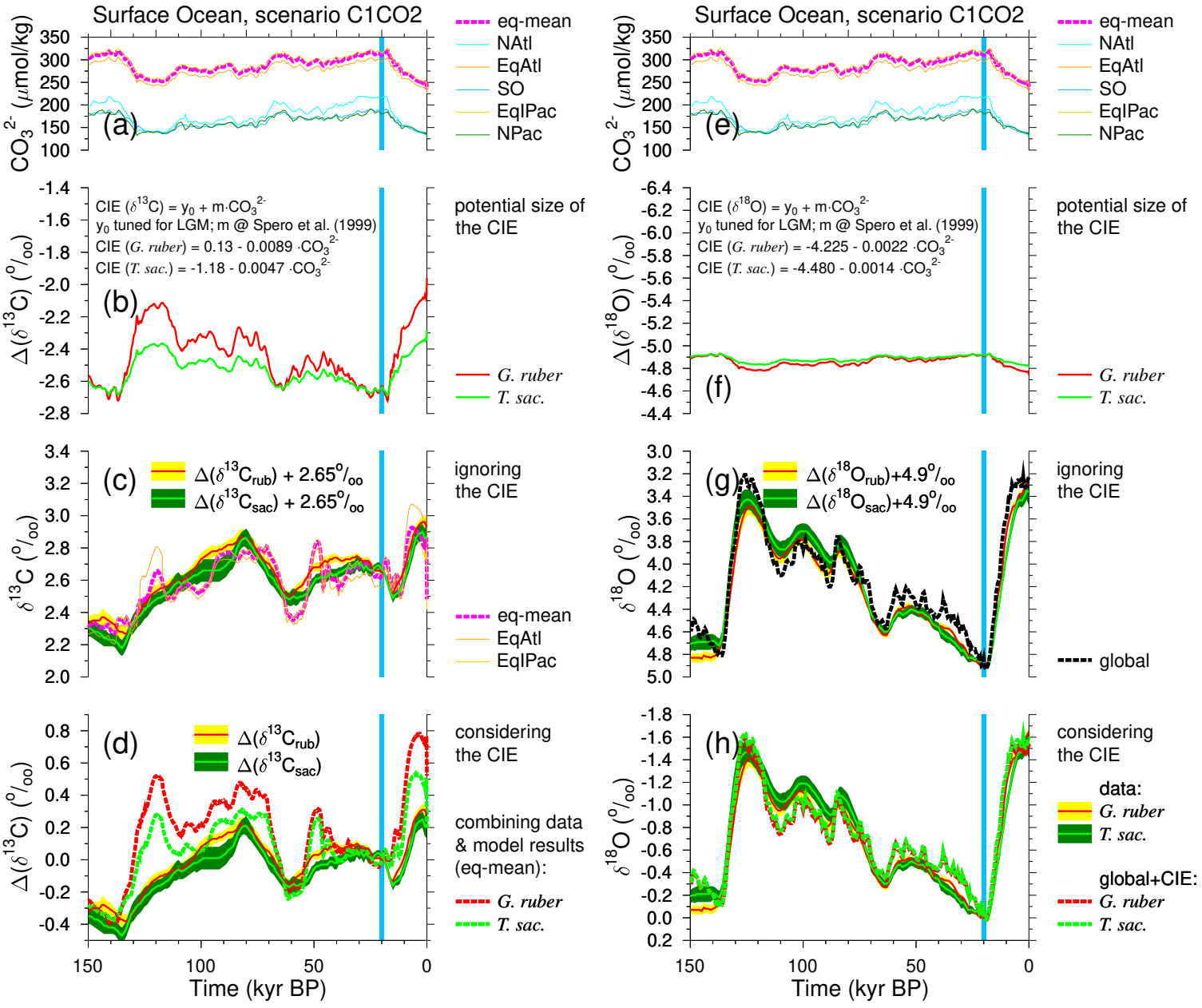

Figure 8. Calculating the suggested carbonate ion effects (CIE) on *G. ruber* and *T. sacculifer*. Left: effects on δ^{13}C; Right: effects on δ^{18}O. (a,e) surface ocean [CO_3^{2-}]; (b,f) potential CIE using slopes from Spero et al. (1999) (c,g) surface ocean conditions when ignoring the CIE or (d,h) when considering the CIE. Mean anomalies (±1 SE) of the isotope stacks are calculated with respect to the mean of 21–19 kyr BP (blue vertical band). Simulations use the results from scenario C1CO2. Different surface ocean areas are distinghuished: North Atlantic (NAtl, north of 50°N), equatorial Atlantic (EqAtl, 40°S–50°N), Southern Ocean (SO, south of 40°S), equatorial Indo-Pacific (EqIPac, 40°S–40°N), North Pacific (NPac, north of 40°N). The mean wider tropical ocean in the model is the mean from the equatorial boxes (eq-mean).

background time series of δ^{18}O which represents the signals when not modified by the CIE. Such a mean δ^{18}O in the wider tropical surface ocean should record the same sea-level related variations than the average global ocean, but might differ in the recorded temperature effect, if the change in average wider tropical sea surface temperature differed from the mean ocean temperature (MOT) change. Pöppelmeier et al. (2023) showed that the LGM-to-PRE change in MOT derived from the model-based interpretation of noble gas reconstructions in ice cores is 2.1 ± 0.7 K. The reconstructed rise in MOT is slightly higher when ignoring the effect of past saturation changes on noble gases (Shackleton et al., 2023). The data assimilation effort on LGM temperature changes by Tierney et al. (2020) is broadly in agreement with the MOT change of Pöppelmeier et al. (2023) and proposes that the tropical (30°S to 30°N) sea surface was around 2.6 K colder at LGM than at PRE, agreeing within the uncertainties with the MOT change. To a first order we therefore assume that the planktic foraminifera should record the same temperature effect in δ^{18}O as contained in the mean ocean. Thus, the global ocean δ^{18}O calculated from stacking benthic time series (Lisiecki and Stern, 2016) represents the CIE-free background against which we compare our new $\Delta(\delta^{18}\mathrm{O}_{\mathrm{rub}})$ and $\Delta(\delta^{18}\mathrm{O}_{\mathrm{sac}})$ stacks.

From the simulated LGM-to-PRE change in mean wider tropical surface ocean CO_3^{2-} of about $-70\,\mu$mol kg^{-1} (Figure 8e) and the laboratory-based amplitudes of the CIE (–0.0022 and –0.0014‰ change in δ^{18}O per μmol kg^{-1} for *G. ruber* and *T. sacculifer*, respectively (Spero et al., 1999)), we derived that $\Delta(\delta^{18}\mathrm{O}_{\mathrm{rub}})$ and $\Delta(\delta^{18}\mathrm{O}_{\mathrm{sac}})$ should record the changes since the LGM by +0.15 and +0.10 ‰ differently than how δ^{18}O in the surface waters truly changed (Figure 8f). Compared to the G/IG amplitude in mean ocean δ^{18}O of –1.65‰ (Figure 8g) these potential CIEs represent corrections of –9% and –6%, a difference by 3% which might be difficult to detect in the paleo records. A linear regression through a scatter plat of δ^{18}O + $\mathrm{CIE}_{\mathrm{rub}}$ versus δ^{18}O + $\mathrm{CIE}_{\mathrm{sac}}$ has a slope of 0.97 ($r^2 = 1.00$, Figure S8b), which is indistinguishable from the slope obtained from regression through the data stacks (Figure 6b), while the slope when considering the CIE should move to unity (indicating that both species were recording the same signal underneath the CIE) if the effect plays an important role during data interpretation. The evidences for or against the CIE in δ^{18}O from both data and models are therefore inconclusive.

4 Conclusions

The CIE for δ^{13}C and δ^{18}O recorded in planktic foraminifera was first identified in laboratory experiments (Spero et al., 1997, 1999), and it was, based on theory, suggested for both isotopes that the underlying processes are directly related to the pH in the surrounding sea water during hard shell formation (Zeebe et al., 1999; Zeebe, 1999). However, these theoretical studies were already unable to confirm the full range of the CIE as contained in the experiments. Furthermore, according to Bijma et al. (1999) it is impossible to determine if pH or $[CO_3^{2-}]$ is responsible for the observed fractionation effects. If this theoretical understanding is correct we would expect to see the CIE in neither or both isotopes in the our mono-specific stacks. Thus, although the interpretation of δ^{18}O with respect to the CIE is, due to the signal-to-noise ratio, uncertain we argue, based on the clear evidence of a lack of the CIE in the recording of δ^{13}C in *G. ruber* and *T. sacculifer*, that there is probably also no significant CIE contained in the δ^{18}O time series of both species. This finding argues against the suggestion of Spero et al. (1999), that the CIE and δ^{13}C time series from *G. ruber* and *T. sacculifer* might be used to calculate a record of surface ocean

[CO_3^{2-}]. Furthermore, we suggest to use our new stack of $\Delta(\delta^{13}C_{rub})$ as representative of $\delta^{13}C_{DIC}$ in the wider tropical surface ocean.

Various possible explanations for a lack of a CIE on orbital timescales exist. First, it might be that the isotopic fractionation during hard shell formation in *G. ruber* and *T. sacculifer* is rather insensitive to [CO_3^{2-}] in the range of interest (250–320 μmol kg^{-1}). Such an insensitivity has been suggested for other species (Bijma et al., 1999), but due to a lack of published data — the slopes of the CIE in *G. ruber* and *T. sacculifer* were only summarized in Spero et al. (1999), while underlying experiments have never been published in the peer-reviewed literature — it cannot be properly checked for the two species investigated here. Second, not the CIE, but alternatively the incorporation of respired CO_2 (depleted in $\delta^{13}C$) during shell formation might be responsible for the observed isotope data in laboratory experiments performed with *Orbulina universa* and *Globigerina bulloides* (Bijma et al., 1999). This process might also play a role in *G. ruber* and *T. sacculifer*, but would only explain observed effects in $\delta^{13}C$, but not in $\delta^{18}O$. However, since our stacks are inconclusive with respect to the CIE and $\delta^{18}O$, they might be of relevance here. A third explanation might be related to homeostasis. In symbiont-bearing planktic foraminifera, such as *G. ruber* and *T. sacculifer*, the *p*H at the shell surface critically depends on photosynthesis and hence light levels and symbiont density (Jørgensen et al., 1985). In order to facilitate calcification, *G. ruber* and *T. sacculifer* may actively influence the *p*H at the shell surface by seeking specific (optimum) light levels through vertical migration, thereby keeping the CIE constant over time. Planktic foraminifera are known to move vertically in the water column (e.g. Kimoto, 2015). Vertical migration to optimise both nutrient uptake and light has been proposed to play an important role in phytoplankton by modelling (Wirtz et al., 2022), an effect which recently has been supported by field data (Zheng et al., 2023). We speculate similar behaviour could occur in the two planktic foraminifera species. Indeed, Jonkers and Kučera (2017) and Daëron and Gray (2023) found that $\delta^{18}O$ in various planktic foraminifera (including *G. ruber* and *T. sacculifer*) is best explained by also considering calcification in waters deeper than their expected living depth.

It is too early to able able to generalise our finding that on orbital timescales the CIE plays no role for the interpretation of signals in planktic foraminifera in paleo records. For that effort more mono-specific stacks are necessary, preferable from conceptually different foraminifera species without symbionts or spines, as these might potentially show a different behaviour with respect to light (and *p*H) optimisation. However, our findings might suggest that previous studies on planktic $\delta^{13}C$, which ignored the CIE (e.g. Lynch-Stieglitz et al., 2019; Lund et al., 2019) might not be biased.

Our carbon cycle simulations confirm that atmospheric $\delta^{13}CO_2$ and mean surface ocean $\delta^{13}C_{DIC}$ are tightly related to each other, highlighting the importance of air-sea gas exchange for carbon isotopes. This is not entirely new and has already been discussed before (e.g. Lynch-Stieglitz et al., 2019; Shao et al., 2021; Pinho et al., 2023). However, the ^{13}C cycle is more complex than stated previously (Lynch-Stieglitz et al., 2019; Hu et al., 2020; Pinho et al., 2023) which suggest that one might calculate a mean surface ocean $\delta^{13}C_{DIC}$ as function of atmospheric $\delta^{13}CO_2$ and a temperature-dependent fractionation during gas exchange. We here assumed, based on modern data from Verwega et al. (2021), that species composition and therefore isotopic fractionation during marine photosynthesis might also be temperature-dependent having an important impact on surface ocean $\delta^{13}C_{DIC}$. Furthermore, our simulation results show that $\delta^{13}C_{DIC}$ in polar and wider tropical surface ocean have a different and time-dependent relation to atmospheric $\delta^{13}CO_2$.

Finally, since our simulations were forced by atmospheric carbon records we are unable to identify specific processes being responsible for the simulated changes in the ^{13}C cycle. Recent climate simulations (Yun et al., 2023) emphazise the importance of the 405 kyr eccentricity cycle in tropical hydroclimate. It therefore seems reasonable that the missing long-term variability in $\delta^{13}C$ in our setup might indeed be connected to weathering fluxes as proposed before (e.g. Schneider et al., 2013; Wang et al., 2014), something which needs to be tested in more detail in future carbon cycle simulation studies.

Code and data availability. PaleoDataView, used for data processing (Langner and Mulitza, 2019), is available at https://www.marum.de/Dr.-stefan-mulitza/PaleoDataView.html (last access 16 Nov 2023). In Table S1 meta data on the data selction are contained, which includes references to the original publications. The reference list based on citations in the Supplements (Table S1) is separately attached to the end of the main text. Most of the data from the planktic foraminifera *G. ruber* and *T. sacculifer* are already contained in the World Atlas of late Quaternary Foraminiferal Oxygen and Carbon Isotope Ratios (Mulitza et al., 2021; Mulitza et al., 2022). The data sets not yet contained in the World Atlas are Duplessy (1982); CLIMAP Project Members (1994); Meinecke (1999) and from three theses (Zahn-Knoll, 1986; Slowey, 1990; Romahn, 2014), from which data have been manually extraced from Tables within the theses. Simulation results and the data contributing to our data compilation including raw data, the Bacon settings and a netCDF file of the PaleoDataView Collection are available from PANGAEA (Köhler and Mulitza, 2023). Data for atmospheric CO_2 and $\delta^{13}CO_2$ are found in Eggleston et al. (2016b); Köhler et al. (2017b); Menking et al. (2022a). The stack of deep Pacific benthic $\delta^{13}C$ is contained in Köhler (2022).

Author contributions. PK designed the study, performed the simulations, analysed the data and led the writing of the draft. SM compiled marine $\delta^{13}C$ data and contributed to the writing of the draft.

Competing interests. The authors declare no competing interests.

Acknowledgements. This work is supported by the German Federal Ministry of Education and Research (BMBF), as Research for Sustainability initiative (FONA); www.fona.de through the PalMod project (grant number: 01LP1922A). We thank P.U. Clark for providing the SST data connected to Barth et al. (2018) and J. Bijma for discussions.

References

Al-Rousan, S., Pätzold, J., Al-Moghrabi, S., and Wefer, G.: Invasion of anthropogenic CO_2 recorded in planktonic foraminifera from the northern Gulf of Aqaba, International Journal of Earth Sciences, 93, 1066–1076, https://doi.org/10.1007/s00531-004-0433-4, 2004.

Bachan, A., Lau, K. V., Saltzman, M. R., Thomas, E., Kump, L. R., and Payne, J. L.: A model for the decrease in amplitude of carbon isotope excursions across the Phanerozoic, American Journal of Science, 317, 641–676, https://doi.org/10.2475/06.2017.01, 2017.

Barth, A. M., Clark, P. U., Bill, N. S., He, F., and Pisias, N. G.: Climate evolution across the Mid-Brunhes Transition, Climate of the Past, 14, 2071–2087, https://doi.org/10.5194/cp-14-2071-2018, 2018.

Bauska, T. K., Baggenstos, D., Brook, E. J., Mix, A. C., Marcott, S. A., Petrenko, V. V., Schaefer, H., Severinghaus, J. P., and Lee, J. E.: Carbon isotopes characterize rapid changes in atmospheric carbon dioxide during the last deglaciation, Proceedings of the National Academy of Sciences, 113, 3465–3470, https://doi.org/10.1073/pnas.1513868113, 2016.

Bauska, T. K., Brook, E. J., Marcott, S. A., Baggenstos, D., Shackleton, S., Severinghaus, J. P., and Petrenko, V. V.: Controls on Millennial-Scale Atmospheric CO2 Variability During the Last Glacial Period, Geophysical Research Letters, 45, 7731–7740, https://doi.org/10.1029/2018GL077881, 2018.

Bereiter, B., Eggleston, S., Schmitt, J., Nehrbass-Ahles, C., Stocker, T. F., Fischer, H., Kipfstuhl, S., and Chappellaz, J.: Revision of the EPICA Dome C CO_2 record from 800 to 600 kyr before present, Geophysical Research Letters, 42, 542–549, https://doi.org/10.1002/2014GL061957, 2015.

Bijma, J., Spero, H. J., and Lea, D. W.: Reassessing Foraminiferal Stable Isotope Geochemistry: Impact of the Oceanic Carbonate System (Experimental Results), pp. 489–512, Springer Berlin Heidelberg, Berlin, Heidelberg, https://doi.org/10.1007/978-3-642-58646-0_20, https://doi.org/10.1007/978-3-642-58646-0_20, 1999.

Blaauw, M. and Christen, J. A.: Flexible paleoclimate age-depth models using an autoregressive gamma process, Bayesian Analysis, 6, 457 – 474, https://doi.org/10.1214/11-BA618, 2011.

Black, D., Thunell, R., Wejnert, K., and Astor, Y.: Carbon isotope composition of Caribbean Sea surface waters: Response to the uptake of anthropogenic CO2, Geophysical Research Letters, 38, L16 609, https://doi.org/10.1029/2011GL048538, 2011.

Brandenburg, K. M., Rost, B., de Waal, D. B. V., Hoins, M., and Sluijs, A.: Physiological control on carbon fractionation in marine phytoplankton, Biogeosciences, 19, 3305–3315, https://doi.org/10.5194/bg-19-3305-2022, 2022.

Browaeys, J.: Linear fit with both uncertainties in x and in y [code], MATLAB Central File Exchange. https://www.mathworks.com/matlabcentral/fileexchange/45711-linear-fit-with-both-uncertainties-in-x-and-in-y. Last accessed 16th October 2023, 2023.

Buitenhuis, E. T., Le Quéré, C., Bednaršek, N., and Schiebel, R.: Large Contribution of Pteropods to Shallow $CaCO_3$ Export, Global Biogeochemical Cycles, 33, 458–468, https://doi.org/10.1029/2018GB006110, 2019.

Butzin, M., Heaton, T. J., Köhler, P., and Lohmann, G.: A short note on marine reservoir age simulations used in IntCal20, Radiocarbon, 62, 865–871, https://doi.org/10.1017/RDC.2020.9, 2020.

CLIMAP Project Members: CLIMAP 18K Database, IGBP PAGES/World Data Center-A for Paleoclimatology Data Contribution Series # 94-001. NOAA/NGDC Paleoclimatology Program, Boulder CO, USA, [data set], https://www.ncei.noaa.gov/pub/data/paleo/paleocean/climap/climap18/, 1994.

Curry, W. B. and Crowley, T. J.: The $\delta^{13}C$ of equatorial Atlantic surface waters: implications for ice age pCO_2 levels, Paleoceanography, 2, 489–517, https://doi.org/10.1029/PA002i005p00489, 1987.

Daëron , M. and Gray , W. R.: Revisiting Oxygen-18 and Clumped Isotopes in Planktic and Benthic Foraminifera, Paleoceanography and Paleoclimatology, 38, e2023PA004660, https://doi.org/10.1029/2023PA004660, 2023.

Deines, P.: The carbon isotope geochemistry of mantle xenoliths, Earth-Science Reviews, 58, 247 – 278, https://doi.org/10.1016/S0012-8252(02)00064-8, 2002.

Duplessy, J.-C.: (Table 2) Stable carbon and oxygen isotope ratios of Globigerinoides ruber from sediment core MD77-169, PANGAEA, [data set], https://doi.org/10.1594/PANGAEA.726202, 1982.

Eggleston, S., Schmitt, J., Bereiter, B., Schneider, R., and Fischer, H.: Evolution of the stable carbon isotope composition of atmospheric CO_2 over the last glacial cycle, Paleoceanography, 31, 434–452, https://doi.org/10.1002/2015PA002874, 2016a.

Eggleston, S., Schmitt, J., Bereiter, B., Schneider, R., and Fischer, H.: CO_2 concentration and stable isotope ratios of three Antarctic ice cores covering the period from 149.4 - 1.5 kyr before 1950, PANGAEA, [data set], https://doi.org/10.1594/PANGAEA.859181, 2016b.

Eide, M., Olsen, A., Ninnemann, U. S., and Eldevik, T.: A global estimate of the full oceanic ^{13}C Suess effect since the preindustrial, Global Biogeochemical Cycles, 31, 515–534, https://doi.org/10.1002/2016GB005472, 2017.

Emiliani, C.: Pleistocene temperatures, Journal of Geology, 63, 539–578, 1955.

Felis, T., Hinestrosa, G., Köhler, P., and Webster, J. M.: Role of the deglacial buildup of the Great Barrier Reef for the global carbon cycle, Geophysical Research Letters, 49, e2021GL096 495, https://doi.org/10.1029/2021GL096495, 2022.

Fraile, I., Schulz, M., Mulitza, S., and Kucera, M.: Predicting the global distribution of planktonic foraminiera using a dynamic ecosystem model, Biogeosciences, 5, 891–911, 2008.

Ganopolski, A. and Brovkin, V.: Simulation of climate, ice sheets and CO_2 evolution during the last four glacial cycles with an Earth system model of intermediate complexity, Climate of the Past, 13, 1695–1716, https://doi.org/10.5194/cp-13-1695-2017, 2017.

Hauck, J., Zeising, M., Le Quéré, C., Gruber, N., Bakker, D. C. E., Bopp, L., Chau, T. T. T., Gürses, Ö., Ilyina, T., Landschützer, P., Lenton, A., Resplandy, L., Rödenbeck, C., Schwinger, J., and Séférian, R.: Consistency and Challenges in the Ocean Carbon Sink Estimate for the Global Carbon Budget, Frontiers in Marine Science, 7, 852, https://doi.org/10.3389/fmars.2020.571720, 2020.

Heaton, T. J., Köhler, P., Butzin, M., Bard, E., Reimer, R. W., Austin, W. E., Ramsey, C. B., Grootes, P. M., Hughen, K. A., Kromer, B., Reimer, P. J., Adkins, J. F., Burke, A., Cook, M. S., Olsen, J., and Skinner, L. C.: Marine20 - the marine radiocarbon age calibration curve (0 - 55,000 cal BP), simulated data for IntCal20, PANGAEA, [data set], https://doi.org/10.1594/PANGAEA.914500, 2020.

Heaton, T. J., Köhler, P., Butzin, M., Bard, E., Reimer, R. W., Austin, W. E. N., Ramsey, C. B., Grootes, P. M., Hughen, K. A., Kromer, B., Reimer, P. J., Adkins, J., Burke, A., Cook, M. S., Olsen, J., and Skinner, L. C.: Marine20 — the marine radiocarbon age calibration curve (0–55,000 cal BP), Radiocarbon, 62, 779–820, https://doi.org/10.1017/RDC.2020.68, 2020.

Hu, R., Bostock, H. C., Greaves, M., Piotrowski, A. M., and McCave, I. N.: Coupled evolution of stable carbon isotopes between the Southern Ocean and the atmosphere over the last 260 ka, Earth and Planetary Science Letters, 538, 116 215, https://doi.org/10.1016/j.epsl.2020.116215, 2020.

Jonkers, L. and Kučera, M.: Quantifying the effect of seasonal and vertical habitat tracking on planktonic foraminifera proxies, Climate of the Past, 13, 573–586, https://doi.org/10.5194/cp-13-573-2017, 2017.

Jørgensen, B. B., Erez, J., Revsbech, P., and Cohen, Y.: Symbiotic photosynthesis in a planktonic foraminiferan, Globigerinoides sacculifer (Brady), studied with microelectrodes1, Limnology and Oceanography, 30, 1253–1267, https://doi.org/https://doi.org/10.4319/lo.1985.30.6.1253, 1985.

Keeling, C. D.: The Suess effect: ^{13}Carbon-^{14}Carbon interrelations, Environment International, 2, 229 – 300, https://doi.org/10.1016/0160-4120(79)90005-9, 1979.

Khatiwala, S., Schmittner, A., and Muglia, J.: Air-sea disequilibrium enhances ocean carbon storage during glacial periods, Science Advances, 5, eaaw4981, https://doi.org/10.1126/sciadv.aaw4981, 2019.

Kimoto, K.: Planktic Foraminifera, pp. 129–178, Springer Japan, Tokyo, https://doi.org/10.1007/978-4-431-55130-0_7, https://doi.org/10.1007/978-4-431-55130-0_7, 2015.

Köhler, P.: Anthropogenic CO_2 of high emission scenario compensated after 3500 years of ocean alkalinization with an annually constant dissolution of 5 Pg of olivine, Frontiers in Climate, 2, 575 744, https://doi.org/10.3389/fclim.2020.575744, 2020.

Köhler, P.: Plio-Pleistocene simulations from a global carbon cycle box model, PANGAEA, [data set], https://doi.org/10.1594/PANGAEA.940169, 2022.

Köhler, P. and Fischer, H.: Simulating changes in the terrestrial biosphere during the last glacial/interglacial transition, Global and Planetary Change, 43, 33–55, https://doi.org/10.1016/j.gloplacha.2004.02.005, 2004.

Köhler, P. and Mulitza, S.: Mono-specific non-polar stacks of δ^{13}C and δ^{18}O from the planktic foraminifera *G. ruber* and *T. sacculifer* and simulation results of the ^{13}C cycle across the last glacial cycle, PANGAEA, [data set], https://doi.pangaea.de/10.1594/PANGAEA.963761, 2023.

Köhler, P. and Munhoven, G.: Late Pleistocene carbon cycle revisited by considering solid Earth processes, Paleoceanography and Paleoclimatology, 35, e2020PA004 020, https://doi.org/10.1029/2020PA004020, 2020.

Köhler, P., Fischer, H., Munhoven, G., and Zeebe, R. E.: Quantitative interpretation of atmospheric carbon records over the last glacial termination, Global Biogeochemical Cycles, 19, GB4020, https://doi.org/10.1029/2004GB002345, 2005.

Köhler, P., Fischer, H., and Schmitt, J.: Atmospheric $\delta^{13}CO_2$ and its relation to pCO_2 and deep ocean δ^{13}C during the late Pleistocene, Paleoceanography, 25, PA1213, https://doi.org/10.1029/2008PA001703, 2010.

Köhler, P., Nehrbass-Ahles, C., Schmitt, J., Stocker, T. F., and Fischer, H.: A 156 kyr smoothed history of the atmospheric greenhouse gases CO_2, CH_4, and N_2O and their radiative forcing, Earth System Science Data, 9, 363–387, https://doi.org/10.5194/essd-9-363-2017, 2017a.

Köhler, P., Nehrbass-Ahles, C., Schmitt, J., Stocker, T. F., and Fischer, H.: Compilations and splined-smoothed calculations of continuous records of the atmospheric greenhouse gases CO_2, CH_4, and N_2O and their radiative forcing since the penultimate glacial maximum, PANGAEA, [data set], https://doi.org/10.1594/PANGAEA.871273, 2017b.

Köhler, P., Adolphi, F., Butzin, M., and Muscheler, R.: Toward reconciling radiocarbon production rates with carbon cycle changes of the last 55,000 years, Paleoceanography and Paleoclimatology, 37, e2021PA004 314, https://doi.org/10.1029/2021PA004314, 2022.

Langner, M. and Mulitza, S.: Technical note: PaleoDataView — a software toolbox for the collection, homogenization and visualization of marine proxy data, Climate of the Past, 15, 2067–2072, https://doi.org/10.5194/cp-15-2067-2019, 2019.

Laskar, J., Robutel, P., Joutel, F., Gastineau, M., Correia, A. C. M., and Levrard, B.: A long term numerical solution for the insolation quantities of the Earth, Astronomy and Astrophysics, 428, 261–285, https://doi.org/10.1051/0004-6361:20041335, 2004.

Linsley, B. K., Dunbar, R. B., Dassié, E. P., Tangri, N., Wu, H. C., Brenner, L. D., and Wellington, G. M.: Coral carbon isotope sensitivity to growth rate and water depth with paleo-sea level implications, Nature Communications, 10, 2056, https://doi.org/10.1038/s41467-019-10054-x, 2019.

Lisiecki, L. E.: Atlantic overturning responses to obliquity and precession over the last 3 Myr, Paleoceanography, 29, 71–86, https://doi.org/10.1002/2013PA002505, 2014.

Lisiecki, L. E. and Raymo, M. E.: A Pliocene-Pleistocene stack of 57 globally distributed benthic δ^{18}O records, Paleoceanography, 20, PA1003, https://doi.org/10.1029/2004PA001071, 2005.

Lisiecki, L. E. and Stern, J. V.: Regional and global benthic δ^{18}O stacks for the last glacial cycle, Paleoceanography, 31, 1368–1394, https://doi.org/10.1002/2016PA003002, 2016.

Liu, Q., Kandasamy, S., Zhai, W., Wang, H., Veeran, Y., Gao, A., and Chen, C.-T. A.: Temperature is a better predictor of stable carbon isotopic compositions in marine particulates than dissolved CO_2 concentration, Communications Earth & Environment, 3, 303, https://doi.org/10.1038/s43247-022-00627-y, 2022.

Lloyd, J. and Farquhar, G. D.: ^{13}C discrimination during CO_2 assimilation by the terrestrial biosphere, Oecologia, 99, 201–215, 1994.

Lorrain, A., Pethybridge, H., Cassar, N., Receveur, A., Allain, V., Bodin, N., Bopp, L., Choy, C. A., Duffy, L., Fry, B., Goñi, N., Graham, B. S., Hobday, A. J., Logan, J. M., Ménard, F., Menkes, C. E., Olson, R. J., Pagendam, D. E., Point, D., Revill, A. T., Somes, C. J., and Young, J. W.: Trends in tuna carbon isotopes suggest global changes in pelagic phytoplankton communities, Global Change Biology, 26, 458–470, https://doi.org/10.1111/gcb.14858, 2020.

Lund, D., Hertzberg, J., and Lacerra, M.: Carbon isotope minima in the South Atlantic during the last deglaciation: evaluating the influence of air-sea gas exchange, Environmental Research Letters, 14, 055 004, https://doi.org/10.1088/1748-9326/ab126f, 2019.

Lynch-Stieglitz, J., Valley, S. G., and Schmidt, M. W.: Temperature-dependent ocean-atmosphere equilibration of carbon isotopes in surface and intermediate waters over the deglaciation, Earth and Planetary Science Letters, 506, 466 – 475, https://doi.org/10.1016/j.epsl.2018.11.024, 2019.

Ma, W., Tian, J., Li, Q., and Wang, P.: Simulation of long eccentricity (400-kyr) cycle in ocean carbon reservoir during Miocene Climate Optimum: Weathering and nutrient response to orbital change, Geophysical Research Letters, 38, L10 701, https://doi.org/10.1029/2011GL047680, 2011.

Marchal, O., Stocker, T. F., and Joos, F.: A latitude-depth, circulation-biogeochemical ocean model for paleoclimate studies. Development and sensitivities, Tellus, 50B, 290–316, 1998.

Meinecke, G.: Isotopes (G. sacculifer) of sediment core GeoB1112-4, PANGAEA, [data set], https://doi.org/10.1594/PANGAEA.54765, 1999.

Menking, J., Shackleton, S., Barker, S., Bauska, T., Brook, E., Buffen, A., Dyonisius, M., Petrenko, V., and Severinghaus, J.: Taylor Glacier CO_2 Isotope Data 74-59 kyr, U.S. Antarctic Program (USAP) Data Center, [data set], https://doi.org/10.15784/601600, 2022a.

Menking, J. A., Shackleton, S. A., Bauska, T. K., Buffen, A. M., Brook, E. J., Barker, S., Severinghaus, J. P., Dyonisius, M. N., and Petrenko, V. V.: Multiple carbon cycle mechanisms associated with the glaciation of Marine Isotope Stage 4, Nature Communications, 13, 5443, https://doi.org/10.1038/s41467-022-33166-3, 2022b.

Menviel, L., Joos, F., and Ritz, S.: Simulating atmospheric CO_2, ^{13}C and the marine carbon cycle during the Last Glacial-Interglacial cycle: possible role for a deepening of the mean remineralization depth and an increase in the oceanic nutrient inventory, Quaternary Science Reviews, 56, 46 – 68, https://doi.org/10.1016/j.quascirev.2012.09.012, 2012.

Menviel, L., Mouchet, A., Meissner, K. J., Joos, F., and England, M. H.: Impact of oceanic circulation changes on atmospheric $\delta^{13}CO_2$, Global Biogeochemical Cycles, 29, 1944–1961, https://doi.org/10.1002/2015GB005207, 2015.

Mojica Prieto, F. J. and Millero, F. J.: The values of $pK_1 + pK_2$ for the dissolution of carbonic acid in seawater, Geochimica et Cosmochimica Acta, 66, 2529–2540, https://doi.org/10.1016/S0016-7037(02)00855-4, 2002.

Mulitza, S., Bickert, T., Bostock, H. C., Chiessi, C. M., Donner, B., Govin, A., Harada, N., Huang, E., Johnstone, H. J. H., Kuhnert, H., Langner, M., Lamy, F., Lembke-Jene, L., Lisiecki, L. E., Lynch-Stieglitz, J., Max, L., Mohtadi, M., Mollenhauer, G., Muglia, J., Nürnberg, D., Paul, A., Rühlemann, C., Repschläger, J., Saraswat, R., Schmittner, A., Sikes, E. L., Spielhagen, R. F., and Tiedemann, R.:

World Atlas of late Quaternary Foraminiferal Oxygen and Carbon Isotope Ratios (WA_Foraminiferal_Isotopes_2022), PANGAEA, [data set], https://doi.org/10.1594/PANGAEA.936747, 2021.

Mulitza, S., Bickert, T., Bostock, H. C., Chiessi, C. M., Donner, B., Govin, A., Harada, N., Huang, E., Johnstone, H., Kuhnert, H., Langner, M., Lamy, F., Lembke-Jene, L., Lisiecki, L., Lynch-Stieglitz, J., Max, L., Mohtadi, M., Mollenhauer, G., Muglia, J., Nürnberg, D., Paul, A., Rühlemann, C., Repschläger, J., Saraswat, R., Schmittner, A., Sikes, E. L., Spielhagen, R. F., and Tiedemann, R.: World Atlas of late Quaternary Foraminiferal Oxygen and Carbon Isotope Ratios, Earth System Science Data, 14, 2553–2611, https://doi.org/10.5194/essd-14-2553-2022, 2022.

Munhoven, G.: Modelling glacial-interglacial atmospheric CO_2 variations: the role of continental weathering, Ph.D. thesis, Université de Liège, Liège, Belgium, http://hdl.handle.net/2268/161314, 1997.

Munhoven, G. and François, L. M.: Glacial-interglacial variability of atmospheric CO_2 due to changing continental silicate rock weathering: a model study, Journal of Geophysical Research, 101(D16), 21 423–21 437, https://doi.org/10.1029/96JD01842, 1996.

Nederbragt, A. J.: The Effect of Seawater Carbonate Chemistry on the Stable Isotope Composition of Cibicidoides wuellerstorfi and Other Cibicidoides Species, Paleoceanography and Paleoclimatology, 38, e2023PA004 667, https://doi.org/10.1029/2023PA004667, 2023.

Oliver, K. I. C., Hoogakker, B. A. A., Crowhurst, S., Henderson, G. M., Rickaby, R. E. M., Edwards, N. R., and Elderfield, H.: A synthesis of marine sediment core δ^{13}C data over the last 150 000 years, Climate of the Past, 6, 645–673, https://doi.org/10.5194/cp-6-645-2010, 2010.

Oppo, D. W. and Fairbanks, R. G.: Carbon isotope composition of tropcial surface water during the past 22,000 years, Paleoceanography, 4, 333–351, https://doi.org/10.1029/PA004i004p00333, 1989.

Paillard, D.: The Plio-Pleistocene climatic evolution as a consequence of orbital forcing on the carbon cycle, Climate of the Past, 13, 1259–1267, https://doi.org/10.5194/cp-13-1259-2017, 2017.

Pälike, H., Norris, R. D., Herrle, J. O., Wilson, P. A., Coxall, H. K., Lear, C. H., Shackleton, N. J., k. Tripati, A., and Wade, B. S.: The heartbeat of the Oligocene climate system, Science, 314, 1894–1898, doi: 10.1126/science.1133 822, 2006.

Peterson, C. D. and Lisiecki, L. E.: Deglacial carbon cycle changes observed in a compilation of 127 benthic δ^{13}C time series (20–6 ka), Climate of the Past, 14, 1229–1252, https://doi.org/10.5194/cp-14-1229-2018, 2018.

Peterson, C. D., Lisiecki, L. E., and Stern, J. V.: Deglacial whole-ocean δ^{13}C change estimated from 480 benthic foraminiferal records, Paleoceanography, 29, 549–563, https://doi.org/10.1002/2013PA002552, 2014.

Pinho, T., Chiessi, C. M., Campos, M. C., Portilho-Ramos, R. C., Martínez-Méndez, G., Venancio, I. M., Nascimento, R. A., Crivellari, S., Albuquerque, A. L., Arz, H. W., Tiedemann, R., Bahr, A., and Mulitza, S.: Thermodynamic air-sea equilibration controls carbon isotopic composition of the South Atlantic thermocline during the last glacial period, Global and Planetary Change, 229, 104 223, https://doi.org/10.1016/j.gloplacha.2023.104223, 2023.

Pöppelmeier, F., Baggenstos, D., Grimmer, M., Liu, Z., Schmitt, J., Fischer, H., and Stocker, T. F.: The Effect of Past Saturation Changes on Noble Gas Reconstructions of Mean Ocean Temperature, Geophysical Research Letters, 50, e2022GL102 055, https://doi.org/https://doi.org/10.1029/2022GL102055, 2023.

R Core Team: R: A Language and Environment for Statistical Computing, R Foundation for Statistical Computing, Vienna, Austria, https://www.R-project.org, 2023.

Reimer, P. J., Austin, W. E. N., Bard, E., Bayliss, A., Blackwell, P. G., Bronk Ramsey, C., Butzin, M., Cheng, H., Edwards, R. L., Friedrich, M., Grootes, P. M., Guilderson, T. P., Hajdas, I., Heaton, T. J., Hogg, A. G., Hughen, K. A., Kromer, B., Manning, S. W., Muscheler, R., Palmer, J. G., Pearson, C., van der Plicht, H., Reimer, R. W., Richards, D. A., Scott, E. M., Southon, J. R., Turney, C. S. M., Wacker, L.,

Adophi, F., Büntgen, U., Capano, M., Fahrni, S., Fogtmann-Schulz, A., Friedrich, R., Köhler, P., Kudsk, S., Miyake, F., Olsen, J., Reinig, F., Sakamoto, M., Sookdeo, A., and Talamo, S.: The IntCal20 Northern Hemisphere radiocarbon age calibration curve (0–55 cal kBP), Radiocarbon, 62, 725–757, https://doi.org/10.1017/RDC.2020.41, 2020.

Rohde, R. A. and Hausfather, Z.: The Berkeley Earth Land/Ocean Temperature Record, Earth System Science Data, 12, 3469—3479, 2020.

Romahn, S.: Western Indian Ocean circulation and climate variability on different time scales: a study based on stable oxygen and carbon isotopes, benthic foraminiferal assemblages and Mg/Ca paleothermometry, PhD thesis, Fachbereich Geowissenschaften, Universität Bremen, 95 pp., 2014.

Roth, R. and Joos, F.: Model limits on the role of volcanic carbon emissions in regulating glacial-interglacial CO_2 variations, Earth and Planetary Science Letters, 329 - 330, 141 – 149, https://doi.org/10.1016/j.epsl.2012.02.019, 2012.

Rubino, M., Etheridge, D. M., Trudinger, C. M., Allison, C. E., Battle, M. O., Langenfelds, R. L., Steele, L. P., Curran, M., Bender, M., White, J. W. C., Jenk, T. M., Blunier, T., and Francey, R. J.: A revised 1000-year atmospheric δ^{13}C-CO_2 record from Law Dome and South Pole, Antarctica, Journal of Geophysical Research: Atmospheres, 118, 8482–8499, https://doi.org/10.1002/jgrd.50668, 2013.

Russon, T., Paillard, D., and Elliot, M.: Potential origins of 400-500 kyr periodicities in the ocean carbon cycle: A box model approach, Global Biogeochemical Cycles, 24, GB2013, https://doi.org/doi: 10.1029/2009GB003586, 2010.

Schmitt, J., Schneider, R., Elsig, J., Leuenberger, D., Lourantou, A., Chappellaz, J., Köhler, P., Joos, F., Stocker, T. F., Leuenberger, M., and Fischer, H.: Carbon isotope constraints on the deglacial CO_2 rise from ice cores, Science, 336, 711–714, https://doi.org/10.1126/science.1217161, 2012.

Schmittner, A., Gruber, N., Mix, A. C., Key, R. M., Tagliabue, A., and Westberry, T. K.: Biology and air-sea gas exchange controls on the distribution of carbon isotope ratios (δ^{13}C) in the ocean, Biogeosciences, 10, 5793–5816, https://doi.org/10.5194/bg-10-5793-2013, 2013.

Schmittner, A., Bostock, H. C., Cartapanis, O., Curry, W. B., Filipsson, H. L., Galbraith, E. D., Gottschalk, J., Herguera, J. C., Hoogakker, B., Jaccard, S. L., Lisiecki, L. E., Lund, D. C., Martínez-Méndez, G., Lynch-Stieglitz, J., Mackensen, A., Michel, E., Mix, A. C., Oppo, D. W., Peterson, C. D., Repschläger, J., Sikes, E. L., Spero, H. J., and Waelbroeck, C.: Calibration of the carbon isotope composition (δ^{13}C) of benthic foraminifera, Paleoceanography, 32, 512–530, https://doi.org/10.1002/2016PA003072, 2017.

Schneider, R., Schmitt, J., Köhler, P., Joos, F., and Fischer, H.: A reconstruction of atmospheric carbon dioxide and its stable carbon isotopic composition from the penultimate glacial maximum to the last glacial inception, Climate of the Past, 9, 2507–2523, https://doi.org/10.5194/cp-9-2507-2013, 2013.

Shackleton, S., Seltzer, A., Baggenstos, D., and Lisiecki, L. E.: Benthic δ^{18}O records Earth's energy imbalance, Nature Geoscience, 16, 797–802, https://doi.org/10.1038/s41561-023-01250-y, 2023.

Shao, J., Stott, L. D., Menviel, L., Ridgwell, A., Ödalen, M., and Mohtadi, M.: The atmospheric bridge communicated the δ^{13}C decline during the last deglaciation to the global upper ocean, Climate of the Past, 17, 1507–1521, https://doi.org/10.5194/cp-17-1507-2021, 2021.

Slowey, N. C.: The modern and glacial thermoclines along the Bahama Banks, PhD thesis, Massachusetts Institute of Technology and Woods Hole Oceanographic Institution, 1990.

Smith, H. J., Fischer, H., Wahlen, M., Mastroianni, D., and Deck, B.: Dual modes of the carbon cycle since the Last Glacial Maximum, Nature, 400, 248–250, 1999.

Spero, H. J.: Do planktic foraminifera accurately record shifts in the carbon isotopic composition of seawater ΣCO2?, Marine Micropaleontology, 19, 275–285, https://doi.org/https://doi.org/10.1016/0377-8398(92)90033-G, 1992.

Spero, H. J. and Lea, D. W.: Intraspecific stable isotope variability in the planktic foraminiferaGlobigerinoides sacculifer: Results from laboratory experiments, Marine Micropaleontology, 22, 221–234, https://doi.org/https://doi.org/10.1016/0377-8398(93)90045-Y, 1993.

Spero, H. J. and Williams, D. F.: Extracting environmental information from planktonic foraminiferal δ13C data, Nature, 335, 717–719, https://doi.org/10.1038/335717a0, 1988.

Spero, H. J. and Williams, D. F.: Opening the carbon isotope "vital effect" black box 1. Seasonal temperatures in the euphotic zone, Paleoceanography, 4, 593–601, https://doi.org/https://doi.org/10.1029/PA004i006p00593, 1989.

Spero, H. J., Lerche, I., and Williams, D. F.: Opening the carbon isotope 'vital effect' black box, 2, Quantitative model for interpreting foraminiferal carbon isotope data, Paleoceanography, 6, 639–655, https://doi.org/10.1029/91PA02022, 1991.

Spero, H. J., Bijma, J., Lea, D. W., and Bemis, B. E.: Effect of seawater carbonate concentration on foraminiferal carbon and oxygen isotopes, Nature, 390, 497–500, https://doi.org/10.1038/37333, 1997.

Spero, H. J., Bijma, J., Lea, D. W., and Russell, A. D.: Deconvolving Glacial Ocean Carbonate Chemistry from the Planktonic Foraminifera Carbon Isotope Record, in: Reconstructing Ocean History: A Window into the Future, edited by Abrantes, F. and Mix, A. C., pp. 329–342, Springer US, Boston, MA, https://doi.org/10.1007/978-1-4615-4197-4_19, 1999.

The MathWorks Inc.: MATLAB Version: 9.14.0.2206163 (R2023a), Natick, Massachusetts, United States, https://www.mathworks.com, 2023.

Tierney, J. E., Zhu, J., King, J., Malevich, S. B., Hakim, G. J., and Poulsen, C. J.: Glacial cooling and climate sensitivity revisited, Nature, 584, 569–573, https://doi.org/10.1038/s41586-020-2617-x, 2020.

Verwega, M.-T., Somes, C. J., Schartau, M., Tuerena, R. E., Lorrain, A., Oschlies, A., and Slawig, T.: Description of a global marine particulate organic carbon-13 isotope data set, Earth System Science Data, 13, 4861–4880, https://doi.org/10.5194/essd-13-4861-2021, 2021.

Vogel, J. C.: Variability of carbon isotope fractionation during photosynthesis, in: Stable isotopes and plant carbon–water relations, edited by Ehleringer, J. R., Hall, A. E., and Farquhar, G. D., pp. 29–46, Academic Press, San Diego, USA, 1993.

Wang, P., Li, Q., Tian, J., Jian, Z., Liu, C., Li, L., and Ma, W.: Long-term cycles in the carbon reservoir of the Quaternary ocean: a perspective from the South China Sea, National Science Review, 1, 119–143, https://doi.org/10.1093/nsr/nwt028, 2014.

Wirtz, K., Smith, S. L., Mathis, M., and Taucher, J.: Vertically migrating phytoplankton fuel high oceanic primary production, Nature Climate Change, 12, 750–756, https://doi.org/10.1038/s41558-022-01430-5, 2022.

Wolf-Gladrow, D. A., Bijma, J., and Zeebe, R. E.: Model simulation of the carbonate chemistry in the microenvironment of symbiont bearing foraminifera, Marine Chemistry, 64, 181–198, https://doi.org/10.1016/S0304-4203(98)00074-7, 1999.

Young, J. N., Bruggeman, J., Rickaby, R. E. M., Erez, J., and Conte, M.: Evidence for changes in carbon isotopic fractionation by phytoplankton between 1960 and 2010, Global Biogeochemical Cycles, 27, 505–515, https://doi.org/https://doi.org/10.1002/gbc.20045, 2013.

Yun, K.-S., Timmermann, A., Lee, S.-S., Willeit, M., Ganopolski, A., and Jadhav, J.: A transient coupled general circulation model (CGCM) simulation of the past 3 million years, Climate of the Past, 19, 1951–1974, https://doi.org/10.5194/cp-19-1951-2023, 2023.

Zahn-Knoll, R.: Spätquatäre Entwicklung von Küstenauftrieb und Tiefenwasserzirkulation im Nordost-Atlantik. Rekonstruktion anhand stabiler Isotope kalkschaliger Foraminiferen, PhD thesis, Christian-Albrechts-Universität zu Kiel, 111 pp., 1986.

Zeebe, R. E.: An explanation of the effect of seawater carbonate concentration on foraminiferal oxygen isotopes, Geochimica et Cosmochimica Acta, 63, 2001–2007, https://doi.org/10.1016/S0016-7037(99)00091-5, 1999.

Zeebe, R. E. and Wolf-Gladrow, D. A.: CO_2 in Seawater: Equilibrium, Kinetics, Isotopes, vol. 65 of *Elsevier Oceanography Book Series*, Elsevier Science Publishing, Amsterdam, The Netherlands, 2001.

Zeebe, R. E., Bijma, J., and Wolf-Gladrow, D. A.: A diffusion-reaction model of carbon isotope fractionation in foraminifera, Marine Chemistry, 64, 199–227, https://doi.org/10.1016/S0304-4203(98)00075-9, 1999.

Zeebe, R. E., Bijma, J., Hönisch, B., Sanyal, A., Spero, H. J., and Wolf-Gladrow, D. A.: Vital effects and beyond: a modelling perspective on developing palaeoceanographical proxy relationships in foraminifera, in: Biogeochemical Controls on Palaeoceanographic Environmental Proxies, Geological Society of London, https://doi.org/10.1144/SP303.4, 2008.

Zhang, J., Quay, P. D., and Wilbur, D. O.: Carbon isotope fractionation during gas-water exchange and dissolution of CO_2, Geochimica et Cosmochimica Acta, 59, 107–114, 1995.

Zheng, B., Lucas, A. J., Franks, P. J. S., Schlosser, T. L., Anderson, C. R., Send, U., Davis, K., Barton, A. D., and Sosik, H. M.: Dinoflagellate vertical migration fuels an intense red tide, Proceedings of the National Academy of Sciences, 120, e2304590 120, https://doi.org/10.1073/pnas.2304590120, 2023.

Ziveri, P., Stoll, H., Probert, I., Klaas, C., Geisen, M., Ganssen, G., and Young, J.: Stable isotope 'vital effects' in coccolith calcite, Earth and Planetary Science Letters, 210, 137–149, https://doi.org/https://doi.org/10.1016/S0012-821X(03)00101-8, 2003.

Original references of the data contributing to our stacks (cited in Table S1 of the Supplement)

Adegbie, A., Schneider, R., Röhl, U., and Wefer, G.: Glacial millennial-scale fluctuations in central African precipitation recorded in terrigenous sediment supply and freshwater signals offshore Cameroon, Palaeogeography, Palaeoclimatology, Palaeoecology, 197, 323–333, https://doi.org/10.1016/S0031-0182(03)00474-7, 2003.

Adegbie, A. T.: Reconstruction of paleoenvironmental conditions in Equatorial Atlantic and the Gulf of Guinea Basins for the last 245.000 years., PhD thesis, Berichte aus dem Fachbereich Geowissenschaften der Universität Bremen, 178, 113 pp., 2001.

Andres, M. S.: Late quaternary paleoceanography of the Great Australian Bight: A geochemical and sedimentological study of cool-water carbonates, ODP Leg 182, Site 1127, PhD thesis, Swiss Federal Institute of Technology Zurich, Switzerland, 2002.

Arz, H. W., Pätzold, J., and Wefer, G.: Correlated Millennial-Scale Changes in Surface Hydrography and Terrigenous Sediment Yield Inferred from Last-Glacial Marine Deposits off Northeastern Brazil, Quaternary Research, 50, 157–166, https://doi.org/10.1006/qres.1998.1992, 1998.

Arz, H. W., Pätzold, J., and Wefer, G.: The deglacial history of the western tropical Atlantic as inferred from high resolution stable isotope records off northeastern Brazil, Earth and Planetary Science Letters, 167, 105–117, https://doi.org/10.1016/S0012-821X(99)00025-4, 1999a.

Arz, H. W., Pätzold, J., and Wefer, G.: Climatic changes during the last deglaciation recorded in sediment cores from the northeastern Brazilian Continental Margin, Geo-Marine Letters, 19, 209–218, https://doi.org/10.1007/s003670050111, 1999b.

Ausin, B., Haghipour, N., Wacker, L., Voelker, A. H. L., Hodell, D., Magill, C., Looser, N., Bernasconi, S. M., and Eglinton, T. I.: Radiocarbon Age Offsets Between Two Surface Dwelling Planktonic Foraminifera Species During Abrupt Climate Events in the SW Iberian Margin, Paleoceanography and Paleoclimatology, 34, 63–78, https://doi.org/10.1029/2018PA003490, 2019.

Bostock, H. C., Opdyke, B. N., Gagan, M. K., and Fifield, L. K.: Carbon isotope evidence for changes in Antarctic Intermediate Water circulation and ocean ventilation in the southwest Pacific during the last glaciation, Paleoceanography, 19, PA4013, doi: 10.1029/2004PA001 047, 2004.

Chen, M.-T., Shiau, L.-J., Yu, P.-S., Chiu, T.-C., Chen, Y.-G., and Wei, K.-Y.: 500 000-Year records of carbonate, organic carbon, and foraminiferal sea-surface temperature from the southeastern South China Sea (near Palawan Island), Palaeogeography, Palaeoclimatology, Palaeoecology, 197, 113–131, https://doi.org/10.1016/S0031-0182(03)00389-4, 2003.

CLIMAP Project Members: Seasonal reconstructions of the earth's surface at the last glacial maximum, Map and chart series (Geological Society of America), Geological Society of America, Boulder, Colo., 1981.

Curry, W. B. and Crowley, T. J.: The δ^{13}C of equatorial Atlantic surface waters: implications for ice age pCO$_2$ levels, Paleoceanography, 2, 489–517, https://doi.org/10.1029/PA002i005p00489, 1987.

Curry, W. B., Marchitto, T. M., Mcmanus, J. F., Oppo, D. W., and Laarkamp, K. L.: Millennial-scale Changes in Ventilation of the Thermocline, Intermediate, and Deep Waters of the Glacial North Atlantic, vol. 112 of *Geophysical Monograph Series*, pp. 59–76, American Geophysical Union (AGU), https://doi.org/10.1029/GM112p0059, 1999.

De Deckker, P., Moros, M., Perner, K., and Jansen, E.: Influence of the tropics and southern westerlies on glacial interhemispheric asymmetry, Nature Geoscience, 5, 266–269, https://doi.org/10.1038/ngeo1431, 2012.

Duplessy, J.: North Atlantic deep water circulation during the last climate cycle, Bulletin de l'Institut de Geologie du Bassin d'Aquitaine, 31, 371–391, 1982.

Duplessy, J., Bard, E., Arnold, M., Shackleton, N., Duprat, J., and Labeyrie, L.: How fast did the ocean—atmosphere system run during the last deglaciation?, Earth and Planetary Science Letters, 103, 27–40, https://doi.org/10.1016/0012-821X(91)90147-A, 1991.

Dupont, L. and Kuhlmann, H.: Glacial-interglacial vegetation change in the Zambezi catchment, Quaternary Science Reviews, 155, 127–135, https://doi.org/10.1016/j.quascirev.2016.11.019, 2017.

Dürkoop, A.: Der Brasil-Strom im Spatquartär: Rekonstruktion der oberflächennahen Hydrographie während der letzten 400 000 Jahre, PhD thesis, Berichte aus dem Fachbereich Geowissenschaften der Universität Bremen, 119, 121 pp., 1998.

Dürkoop, A., Hale, W., Mulitza, S., Pätzold, J., and Wefer, G.: Stable isotope data of sediment core GeoB1503-1, PANGAEA, [data set], https://doi.org/10.1594/PANGAEA.223482, 1997a.

Dürkoop, A., Hale, W., Mulitza, S., Pätzold, J., and Wefer, G.: Stable isotope data of sediment core GeoB2125-1, PANGAEA, [data set], https://doi.org/10.1594/PANGAEA.223488, 1997b.

Dürkoop, A., Hale, W., Mulitza, S., Pätzold, J., and Wefer, G.: Stable isotope data of sediment core GeoB2202-4, PANGAEA, [data set], https://doi.org/10.1594/PANGAEA.223489, 1997c.

Dyez, K. A., Zahn, R., and Hall, I. R.: Multicentennial Agulhas leakage variability and links to North Atlantic climate during the past 80,000 years, Paleoceanography, 29, 1238–1248, https://doi.org/10.1002/2014PA002698, 2014.

Freimüller, J.: Eine hochauflösende planktische Isotopenaufzeichnung des Heinrich Event 1 im tropischen Südamerika, Bachelor thesis, Fachbereich Geowissenschaften, Universität Bremen, 2013.

Ge, H., Li, Q., and Cheng, X.: Late Quaternary high resolution monsoon records in planktonic stable isotopes from northern South China Sea(in Chinese), Earth Sci: J China Uni Geosci, 35, 515–525, https://doi.org/10.3799/dqkx.2010.000, 2010.

Gemmeke, B.: Spätquartäre Variationen der Sauerstoffisotopen-Zusammensetztung des Oberflächenwassers im östlichen tropischen Nordatlantik, Bachelor thesis, Fachbereich Geowissenschaften, Universität Bremen, 2010.

Gibbons, F. T., Oppo, D. W., Mohtadi, M., Rosenthal, Y., Cheng, J., Liu, Z., and Linsley, B. K.: Deglacial δ^{18}O and hydrologic variability in the tropical Pacific and Indian Oceans, Earth and Planetary Science Letters, 387, 240–251, https://doi.org/10.1016/j.epsl.2013.11.032, 2014.

Gingele, F., De Deckker, P., and Norman, M.: Late Pleistocene and Holocene climate of SE Australia reconstructed from dust and river loads deposited offshore the River Murray Mouth, Earth and Planetary Science Letters, 255, 257–272, https://doi.org/10.1016/j.epsl.2006.12.019, 2007.

Govil, P. and Divakar Naidu, P.: Variations of Indian monsoon precipitation during the last 32 kyr reflected in the surface hydrography of the Western Bay of Bengal, Quaternary Science Reviews, 30, 3871–3879, https://doi.org/10.1016/j.quascirev.2011.10.004, 2011.

Hale, W. and Pflaumann, U.: Stable isotopes on Globigerinoides ruber in sediment core GeoB2109-1, PANGAEA, [data set], https://doi.org/10.1594/PANGAEA.140002, 1999.

Holbourn, A., Kuhnt, W., Kawamura, H., Jian, Z., Grootes, P., Erlenkeuser, H., and Xu, J.: Orbitally paced paleoproductivity variations in the Timor Sea and Indonesian Throughflow variability during the last 460 kyr, Paleoceanography, 20, PA3002, https://doi.org/10.1029/2004PA001094, 2005.

Hou, A., Bahr, A., Raddatz, J., Voigt, S., Greule, M., Albuquerque, A. L., Chiessi, C. M., and Friedrich, O.: Insolation and Greenhouse Gas Forcing of the South American Monsoon System Across Three Glacial-Interglacial Cycles, Geophysical Research Letters, 47, e2020GL087 948, https://doi.org/10.1029/2020GL087948, 2020.

Ivanova, E., Schiebel, R., Singh, A. D., Schmiedl, G., Niebler, H.-S., and Hemleben, C.: Primary production in the Arabian Sea during the last 135 000 years, Palaeogeography, Palaeoclimatology, Palaeoecology, 197, 61–82, https://doi.org/10.1016/S0031-0182(03)00386-9, 2003.

Johnstone, H. J. H., Kiefer, T., Elderfield, H., and Schulz, M.: Calcite saturation, foraminiferal test mass, and Mg/Ca-based temperatures dissolution corrected using XDX—A 150 ka record from the western Indian Ocean, Geochemistry, Geophysics, Geosystems, 15, 781–797, https://doi.org/10.1002/2013GC004994, 2014.

Keigwin, L. D.: Radiocarbon and stable isotope constraints on Last Glacial Maximum and Younger Dryas ventilation in the western North Atlantic, Paleoceanography, 19, PA4012, doi: 10.1029/2004PA001 029, 2004.

Kemle-von Mücke, S.: Oberflächenwasserstruktur und -zirkulation des Südostatlantiks im Spätquartär, PhD thesis, Berichte aus dem Fachbereich Geowissenschaften der Universität Bremen, 55, 151 pp., 1994.

Knaack, J.: Eine neue Transferfunktion zur Rekonstruktion der Paläoproduktivität aus Gemeinschaften mariner Diatomeen, PhD thesis, Geologisch-Paläontologisches Institut und Museum, Christian-Albrechts-Universität Kiel, 119 pp., 1997.

Knaack, J.-J. and Sarnthein, M.: Stable isotopes of foraminifera of ODP Hole 108-658C, PANGAEA, [data set], https://doi.org/10.1594/PANGAEA.227736, 2005.

Kohn, M., Steinke, S., Baumann, K.-H., Donner, B., Meggers, H., and Zonneveld, K. A.: Stable oxygen isotopes from the calcareous-walled dinoflagellate Thoracosphaera heimii as a proxy for changes in mixed layer temperatures off NW Africa during the last 45,000yr, Palaeogeography, Palaeoclimatology, Palaeoecology, 302, 311–322, https://doi.org/10.1016/j.palaeo.2011.01.019, 2011.

Koutavas, A. and Lynch-Stieglitz, J.: Glacial-interglacial dynamics of the eastern equatorial Pacific cold tongue-Intertropical Convergence Zone system reconstructed from oxygen isotope records, Paleoceanography, 18, 1089, https://doi.org/10.1029/2003PA000894, 2003.

Leech, P. J., Lynch-Stieglitz, J., and Zhang, R.: Western Pacific thermocline structure and the Pacific marine Intertropical Convergence Zone during the Last Glacial Maximum, Earth and Planetary Science Letters, 363, 133 – 143, https://doi.org/10.1016/j.epsl.2012.12.026, 2013.

Li, L., Wang, H., Li, J., Zhao, M., and Wang, P.: Changes in sea surface temperature in western South China Sea over the past 450 ka, Chinese Science Bulletin, 54, 3335–3343, https://doi.org/10.1007/s11434-009-0083-9, 2009.

Li, Q., Zheng, F., Chen, M., Xiang, R., Qiao, P., Shao, L., and Cheng, X.: Glacial Paleoceanography off the Mouth of the Mekong River, Southern South China Sea, During the last 500 ka, Quaternary Research, 73, 563–572, https://doi.org/10.1016/j.yqres.2010.03.003, 2010.

Linsley, B. K.: Oxygen-isotope record of sea level and climate variations in the Sulu Sea over the past 150,000 years, Nature, 380, 234–237, https://doi.org/10.1038/380234a0, 1996.

Lo, L., Chang, S.-P., Wei, K.-Y., Lee, S.-Y., Ou, T.-H., Chen, Y.-C., Chuang, C.-K., Mii, H.-S., Burr, G. S., Chen, M.-T., Tung, Y.-H., Tsai, M.-C., Hodell, D. A., and Shen, C.-C.: Nonlinear climatic sensitivity to greenhouse gases over past 4 glacial/interglacial cycles, Scientific Reports, 7, 4626, https://doi.org/10.1038/s41598-017-04031-x, 2017.

Lynch-Stieglitz, J., Polissar, P. J., Jacobel, A. W., Hovan, S. A., Pockalny, R. A., Lyle, M., Murray, R. W., Ravelo, A. C., Bova, S. C., Dunlea, A. G., Ford, H. L., Hertzberg, J. E., Wertman, C. A., Maloney, A. E., Shackford, J. K., Wejnert, K., and Xie, R. C.: Glacial-interglacial changes in central tropical Pacific surface seawater property gradients, Paleoceanography, 30, 423–438, https://doi.org/10.1002/2014PA002746, 2015.

Meinecke, G.: Spätquartäre Oberflächenwassertemperaturen im östlichen äquatorialen Atlantik, PhD thesis, Berichte aus dem Fachbereich Geowissenschaften der Universität Bremen, 29, 181 pp., 1992.

Michael, S., Helmut, E., von Grafenstein, R., and Schroeder, C.: Stable-isotope stratigraphy for the last 750,000 years; Meteor core 13519 from the eastern equatorial Atlantic, Meteor-Forschungsergebnisse Reihe C Geologie und Geophysik, C38, 9–24, 1984.

Mohtadi, M., Lückge, A., Steinke, S., Groeneveld, J., Hebbeln, D., and Westphal, N.: Late Pleistocene surface and thermocline conditions of the eastern tropical Indian Ocean, Quaternary Science Reviews, 29, 887–896, https://doi.org/10.1016/j.quascirev.2009.12.006, 2010a.

Mohtadi, M., Steinke, S., Lückge, A., Groeneveld, J., and Hathorne, E. C.: Glacial to Holocene surface hydrography of the tropical eastern Indian Ocean, Earth and Planetary Science Letters, 292, 89–97, https://doi.org/10.1016/j.epsl.2010.01.024, 2010b.

Mohtadi, M., Oppo, D. W., Steinke, S., Stuut, J.-B. W., De Pol-Holz, R., Hebbeln, D., and Luckge, A.: Glacial to Holocene swings of the Australian-Indonesian monsoon, Nature Geoscience, 4, 540–544, https://doi.org/10.1038/ngeo1209, 2011.

Mohtadi, M., Prange, M., Oppo, D. W., De Pol-Holz, R., Merkel, U., Zhang, X., Steinke, S., and Luckge, A.: North Atlantic forcing of tropical Indian Ocean climate, Nature, 509, 76–80, https://doi.org/10.1038/nature13196, 2014.

Monteagudo, M. M., Lynch-Stieglitz, J., Marchitto, T. M., and Schmidt, M. W.: Central Equatorial Pacific Cooling During the Last Glacial Maximum, Geophysical Research Letters, 48, e2020GL088 592, https://doi.org/10.1029/2020GL088592, 2021.

Moros, M., De Deckker, P., Jansen, E., Perner, K., and Telford, R. J.: Holocene climate variability in the Southern Ocean recorded in a deep-sea sediment core off South Australia, Quaternary Science Reviews, 28, 1932–1940, https://doi.org/10.1016/j.quascirev.2009.04.007, 2009.

Mulitza, S.: Spätquartäre Variationen der oberflächennahen Hydrographie im westlichen äquatorialen Atlantik., PhD thesis, Berichte aus dem Fachbereich Geowissenschaften der Universität Bremen, 57, 95 pp., 1994.

Mulitza, S.: Globigerinoides ruber (white) isotopes of sediment core GeoB2109-1, PANGAEA, [data set], https://doi.org/10.1594/PANGAEA.713179, 2009.

Mulitza, S., Arz, H., von Mücke, S. K., Moss, C., Niebler, H.-S., Pätzold, J., and Segl, M.: The South Atlantic Carbon Isotope record of planktic foraminifera, in: Use of proxies in Paleoceanography: Examples from the South Atlantic, edited by Fischer, G. and Wefer, G., pp. 427–445, Springer Verlag, Berlin, Heidelberg, Germany, https://doi.org/10.1007/978-3-642-58646-0_17, 1999.

Mulitza, S., Bickert, T., Bostock, H. C., Chiessi, C. M., Donner, B., Govin, A., Harada, N., Huang, E., Johnstone, H., Kuhnert, H., Langner, M., Lamy, F., Lembke-Jene, L., Lisiecki, L., Lynch-Stieglitz, J., Max, L., Mohtadi, M., Mollenhauer, G., Muglia, J., Nürnberg, D., Paul, A., Rühlemann, C., Repschläger, J., Saraswat, R., Schmittner, A., Sikes, E. L., Spielhagen, R. F., and Tiedemann, R.: World Atlas of late Quaternary Foraminiferal Oxygen and Carbon Isotope Ratios, Earth System Science Data, 14, 2553–2611, https://doi.org/10.5194/essd-14-2553-2022, 2022.

Naik, S. S. and Naidu, P. D.: Carbonate preservation during the 'mystery interval' in the northern Indian Ocean, Geochemical Journal, 50, 357–362, https://doi.org/10.2343/geochemj.2.0420, 2016.

Parker, A. O., Schmidt, M. W., Jobe, Z. R., and Slowey, N. C.: A new perspective on West African hydroclimate during the last deglaciation, Earth and Planetary Science Letters, 449, 79–88, https://doi.org/10.1016/j.epsl.2016.05.038, 2016.

Patrick, A. and Thunell, R. C.: Tropical Pacific sea surface temperatures and upper water column thermal structure during the Last Glacial Maximum, Paleoceanography, 12, 649–657, https://doi.org/10.1029/97PA01553, 1997.

Paul, A., Reimer, J. J. G., Fürstenau, J., Kinkel, H., and Betzler, C.: Relationship between Late Pleistocene sea-level variations, carbonate platform morphology and aragonite production (Maldives, Indian Ocean), Sedimentology, 59, 1640–1658, https://doi.org/10.1111/j.1365-3091.2011.01319.x, 2012.

Portilho-Ramos, R. C., Cruz, A. P. S., Barbosa, C. F., Rathburn, A. E., Mulitza, S., Venancio, I. M., Schwenk, T., Rühlemann, C., Vidal, L., Chiessi, C. M., and Silveira, C. S.: Methane release from the southern Brazilian margin during the last glacial, Scientific Reports, 8, 5948, https://doi.org/10.1038/s41598-018-24420-0, 2018.

Raza, T., Ahmad, S. M., Sahoo, M., Banerjee, B., Bal, I., Dash, S., Suseela, G., and Mukherjee, I.: Hydrographic changes in the southern Bay of Bengal during the last ∼65,000 y inferred from carbon and oxygen isotopes of foraminiferal fossil shells, Quaternary International, 333, 77–85, https://doi.org/10.1016/j.quaint.2014.02.010, 2014.

Richter, T.: Sedimentary fluxes at the Mid-Atlantic Ridge: sediment sources, accumulation rates, and geochemical characterisation, PhD thesis, GEOMAR-Report, 73, GEOMAR Research Center for Marine Geosciences, Christian-Albrechts-Universität in Kiel, 173 pp., Kiel, https://doi.org/10.3289/GEOMAR_REP_73_1998, 1998.

Romahn, S.: Western Indian Ocean circulation and climate variability on different time scales: a study based on stable oxygen and carbon isotopes, benthic foraminiferal assemblages and Mg/Ca paleothermometry, PhD thesis, Fachbereich Geowissenschaften, Universität Bremen, 95 pp., 2014.

Romahn, S., Mackensen, A., Groeneveld, J., and Pätzold, J.: Deglacial intermediate water reorganization: new evidence from the Indian Ocean, Climate of the Past, 10, 293–303, https://doi.org/10.5194/cp-10-293-2014, 2014.

Rühlemann, C., Frank, M., Hale, W., Mangini, A., Mulitza, S., Müller, P., and Wefer, G.: Late Quaternary productivity changes in the western equatorial Atlantic: Evidence from 230Th-normalized carbonate and organic carbon accumulation rates, Marine Geology, 135, 127–152, https://doi.org/10.1016/S0025-3227(96)00048-5, 1996.

Sarnthein, M., Winn, K., Duplessy, J.-C., and Fontugne, M. R.: Global variations of surface ocean productivity in low and mid latitudes: Influence on CO_2 reservoirs of the deep ocean and atmosphere during the last 21,000 years, Paleoceanography, 3, 361–399, https://doi.org/10.1029/PA003i003p00361, 1988.

Sarnthein, M., Winn, K., Jung, S. J. A., Duplessy, J. C., Labeyrie, L., Erlenkeuser, H., and Ganssen, G.: Changes in East Atlantic deepwater circulation over the last 30,000 years: eight time slice reconstruction, Paleoceanography, 99, 209–268, https://doi.org/10.1029/93PA03301, 1994.

Schefuß, E., Schouten, S., and Schneider, R. R.: Climatic controls on central African hydrology during the past 20,000 years, Nature, 437, 1003–1006, https://doi.org/10.1038/nature03945, 2005.

Schneider, R.: Spätquartäre Produktivitätsänderungen im östlichen Angola-Becken: Reaktion auf Variationen im Passat-Monsun-Windsystem und in der Advektion des Benguela-Küstenstroms, PhD thesis, Berichte aus dem Fachbereich Geowissenschaften der Universität Bremen, 21, 198 pp., Bremen, 1991.

Shackleton, N., Le, J., Mix, A., and Hall, M.: Carbon isotope records from pacific surface waters and atmospheric carbon dioxide, Quaternary Science Reviews, 11, 387–400, https://doi.org/10.1016/0277-3791(92)90021-Y, 1992.

Sirocko, F.: Zur Akkumulation von Staubsedimenten im nördlichen Indischen Ozean, Anzeiger der Klimageschichte Arabiens und Indiens: = Accumulation of eolian sediments in the northern Indian Ocean, record of the climatic history of Arabia and India, PhD thesis, Geolog.-Paläontolog. Inst. u. Museum, Christian-Albrechts-Univity, Kiel, Berichte. 27, 185 pp., 1989.

Sirocko, F., Garbe-Schönberg, D., and Devey, C.: Processes controlling trace element geochemistry of Arabian Sea sediments during the last 25,000 years, Global and Planetary Change, 26, 217–303, https://doi.org/10.1016/S0921-8181(00)00046-1, 2000.

Slowey, N. C.: The modern and glacial thermoclines along the Bahama Banks, PhD thesis, Massachusetts Institute of Technology and Woods Hole Oceanographic Institution, 1990.

Slowey, N. C. and Curry, W. B.: Enhanced ventilation of the North Atlantic subtropical gyre thermocline during the last glaciation, Nature, 358, 665–668, https://doi.org/10.1038/358665a0, 1992.

Spero, H. J., Mielke, K. M., Kalve, E. M., Lea, D. W., and Pak, D. K.: Multispecies approach to reconstructing eastern equatorial Pacific thermocline hydrography during the past 360 ky, Paleoceanography, 18, 1022, https://doi.org/10.1029/2002PA000814, 2003.

Stott, L., Poulsen, C., Lund, S., and Thunell, R.: Super ENSO and Global Climate Oscillations at Millennial Time Scales, Science, 297, 222–226, https://doi.org/10.1126/science.1071627, 2002.

Stott, L., Timmermann, A., and Thunell, R.: Southern hemisphere and deep-sea warming led deglacial atmospheric CO_2 rise and tropical warming, Science, 318, 435–438, doi: 10.1126/science.1143 791, 2007.

Tian, J., Huang, E., and Pak, D. K.: East Asian winter monsoon variability over the last glacial cycle: Insights from a latitudinal sea-surface temperature gradient across the South China Sea, Palaeogeography, Palaeoclimatology, Palaeoecology, 292, 319–324, https://doi.org/10.1016/j.palaeo.2010.04.005, 2010.

Tierney, J. E., deMenocal, P. B., and Zander, P. D.: A climatic context for the out-of-Africa migration, Geology, 45, 1023–1026, https://doi.org/10.1130/G39457.1, 2017.

Toledo, F. A., Costa, K. B., and Pivel, M. A.: Salinity changes in the western tropical South Atlantic during the last 30 kyr, Global and Planetary Change, 57, 383–395, https://doi.org/10.1016/j.gloplacha.2007.01.001, 2007.

Vahlenkamp, M.: The Anatomy of Heinrich Event 1 — A Multiproxy Study of Centennial to Millennial Scale Climate Change off Brazil, Master thesis, Fachbereich Geowissenschaften, Universität Bremen, 2013.

Venancio, I. M., Mulitza, S., Govin, A., Santos, T. P., Lessa, D. O., Albuquerque, A. L. S., Chiessi, C. M., Tiedemann, R., Vahlenkamp, M., Bickert, T., and Schulz, M.: Millennial- to Orbital-Scale Responses of Western Equatorial Atlantic Thermocline Depth to Changes in the Trade Wind System Since the Last Interglacial, Paleoceanography and Paleoclimatology, 33, 1490–1507, https://doi.org/10.1029/2018PA003437, 2018.

von Rad, U., Schulz, H., Riech, V., den Dulk, M., Berner, U., and Sirocko, F.: Multiple monsoon-controlled breakdown of oxygen-minimum conditions during the past 30,000 years documented in laminated sediments off Pakistan, Palaeogeography, Palaeoclimatology, Palaeoecology, 152, 129–161, https://doi.org/10.1016/S0031-0182(99)00042-5, 1999.

Wang, L., Sarnthein, M., Erlenkeuser, H., Grimalt, J., Grootes, P., Heilig, S., Ivanova, E., Kienast, M., Pelejero, C., and Pflaumann, U.: East Asian monsoon climate during the Late Pleistocene: high-resolution sediment records from the South China Sea, Marine Geology, 156, 245–284, https://doi.org/10.1016/S0025-3227(98)00182-0, 1999.

Wang, P., Li, Q., Tian, J., He, J., Jian, Z., Ma, W., and Dang, H.: Monsoon influence on planktic δ^{18}O records from the South China Sea, Quaternary Science Reviews, 142, 26–39, https://doi.org/10.1016/j.quascirev.2016.04.009, 2016.

Wang, Y. V., Leduc, G., Regenberg, M., Andersen, N., Larsen, T., Blanz, T., and Schneider, R. R.: Northern and southern hemisphere controls on seasonal sea surface temperatures in the Indian Ocean during the last deglaciation, Paleoceanography, 28, 619–632, https://doi.org/10.1002/palo.20053, 2013.

Wefer, G., Berger, W. H., Bickert, T., Donner, B., Fischer, G., von Mücke, S. K., Meinecke, G., Müller, P. J., Mulitza, S., Niebler, H.-S., Pätzold, J., Schmidt, H., Schneider, R. R., and Segl, M.: Late Quaternary Surface Circulation of the South Atlantic: The Stable Isotope Record and Implications for Heat Transport and Productivity, pp. 461–502, Springer Berlin Heidelberg, Berlin, Heidelberg, https://doi.org/10.1007/978-3-642-80353-6_25, 1996.

Winn, K.: Density, carbon and stable isotope ratios of foraminifera from sediment core SO35-272, PANGAEA, [data set], in: Winn, Kyaw; Werner, Friedrich; Erlenkeuser, Helmut (2013): Age model and stable isotope ratios of sediment cores from the South China Sea. PANGAEA, https://doi.org/10.1594/PANGAEA.807876, 2013.

Zahn-Knoll, R.: Spätquatäre Entwicklung von Küstenauftrieb und Tiefenwasserzirkulation im Nordost-Atlantik. Rekonstruktion anhand stabiler Isotope kalkschaliger Foraminiferen, PhD thesis, Christian-Albrechts-Universität zu Kiel, 111 pp., 1986.

Zimmermann, R.: Spätquartäre Geschichte der Oberflächenstratifizierung im Golf von Guinea anhand des Schwerelotkernes GeoB 4905-4, Bachelor thesis, Fachbereich Geowissenschaften, Universität Bremen, 2013.